



Geometrically nonlinear isogeometric analysis of functionally graded microplates with the modified couple stress theory



Hoang X. Nguyen^a, Elena Atroshchenko^b, H. Nguyen-Xuan^{c,d,*}, Thuc P. Vo^{a,e,*}

^a Faculty of Engineering and Environment, Northumbria University, Newcastle upon Tyne NE1 8ST, United Kingdom

^b Department of Mechanical Engineering, University of Chile, Santiago 8370448, Chile

^c Department of Physical Therapy, Graduate Institute of Rehabilitation Science, China Medical University, Taichung 40402, Taiwan

^d Department of Architectural Engineering, Sejong University, 209 Neungdong-ro, Gwangjin-gu, Seoul 05006, Republic of Korea

^e Institute of Research and Development, Duy Tan University, 03 Quang Trung, Da Nang, Vietnam

ARTICLE INFO

Article history:

Received 24 April 2017

Accepted 26 July 2017

Available online 17 August 2017

Keywords:

Isogeometric analysis

Modified couple stress theory

Refined plate theory

Nonlinear analysis

Functionally graded microplates

ABSTRACT

In this study, a new and efficient computational approach based on isogeometric analysis (IGA) and refined plate theory (RPT) is proposed for the geometrically nonlinear analysis of functionally graded (FG) microplates. While the microplates' size-dependent effects are efficiently captured by a simple modified couple stress theory (MCST) with only one length scale parameter, the four-unknown RPT is employed to establish the displacement fields which are eventually used to derive the nonlinear von Kármán strains. The NURBS-based isogeometric analysis is used to construct high-continuity elements, which is essentially required in the modified couple stress and refined plate theories, before the iterative Newton-Raphson algorithm is employed to solve the nonlinear problems. The successful convergence and comparison studies as well as benchmark results of the nonlinear analysis of FG microplates ascertain the validity and reliability of the proposed approach. In addition, a number of studies have been carried out to investigate the effects of material length scale, material and geometrical parameters on the nonlinear bending behaviours of microplates.

© 2017 Elsevier Ltd. All rights reserved.

1. Introduction

Classical elasticity has been well established and played a crucial role in the development of the material models and structural responses in various engineering fields ranging from mechanical to bio-engineering. It fundamentally follows the Hooke's law assuming the linear relation between the force and the change in displacement via the stiffness of the body on which the force is applied. However, the classical elasticity fails to capture the size-dependent effects which occur in the small-scale structures. These effects, indeed, have been pointed out by Lam et al. [1] after conducting the experimental bending test of epoxy polymeric microbeams witnessing the bending rigidity was 2.4 times higher as the beam thickness declined from 115 μm to 20 μm . Those small-scale structures have created new challenges in modelling,

for instance, when one attempts to investigate the structural behaviours of elements in micro- and nano-electro-mechanical systems [2,3], carbon nanotube actuators [4], space and bio-engineering [5]. In order to model the materials and structures, the small length scales and its interaction with other particles should be carefully considered. These challenges encourage researchers to focus on a new research topic of modelling of small structures and predicting their behaviours. The theories for more general descriptions of materials' response have been initially developed dating back to the 1960s with the early works of Mindlin [6–8] and Mindlin and Tiersten [9] who developed higher-order theories of elasticity. There has also been a surge of interest in the generalised continuum since then including the development of non-local theory, strain gradient theory and couple stress theory.

The non-local elasticity was initially proposed by Eringen [10] and Eringen and Edelen [11] who assumed that the stress of a point in an elastic body not only depends on the strain at that point but also, theoretically, at all other points in the continuum. While this theory considers the interactions between atoms, it also includes the internal length scale in the constitutive equations as a material parameter [12]. However, as pointed out by Reddy [13], the Eringen's theory appears to be not applicable for the structural

* Corresponding authors at: Department of Physical Therapy, Graduate Institute of Rehabilitation Science, China Medical University, Taichung 40402, Taiwan (H. Nguyen-Xuan). Faculty of Engineering and Environment, Northumbria University, Newcastle upon Tyne NE1 8ST, United Kingdom (T.P. Vo).

E-mail addresses: xuan.h.nguyen@northumbria.ac.uk (H.X. Nguyen), eatroshch@gmail.com (E. Atroshchenko), a28271@mail.cmuh.org.tw (H. Nguyen-Xuan), thuc.vo@northumbria.ac.uk (T.P. Vo).

mechanic problems in which the von Kármán and kinetic energy are involved. Concerning the strain gradient theory, this theory which was pioneered by Fleck et al. [14,15] assumes that the strain energy density depends on the first and second order displacement gradients. In addition, this theory contains the rotation gradient tensor, dilatation tensor, and deviatoric stretch gradient tensor. These assumptions require three material length scale parameters to be used in the strain gradient theory. Mindlin and Toupin are among those who first introduced the ideas of couple stress theory [9,16]. According to their studies, the strength of the continuum body is governed by both strain and curvature. Since it is experimentally difficult to determine all two material length scale parameters as proposed in the classical couple stress theory, models with less number of those parameters were in need to develop. Yang et al. [17] proposed the modified couple stress theory (MCST) which requires only one material length scale parameter in deriving the constitutive equation. In addition, this modification includes a symmetric couple stress tensor. Owing to these striking features, the MCST is continuously developed and has its own extensive literature. Chen and Li [18] developed quadrilateral spline element for couple stress elasticity. The MCST has been also applied to investigate the behaviours of beams with different types of theories including Bernoulli-Euler [19,20], Timoshenko [21] and higher-orders [22,23]. Employing the MCST, a large number of works predicting plates' behaviours has been done for both linear and nonlinear analyses. Tsiatas [24] presented the static analysis of isotropic microplates based on the MCST. While Yin et al. [25] considered the vibrational responses of microplates, an investigation on the behaviours of Mindlin microplates for both stretching effects and bending has been conducted by Ma et al. [26]. Thai and Vo [27] paid their attention to the bending and vibration responses of size-dependent microplates. Reddy and his colleagues worked on the nonlinear finite element analysis (FEA) of FG microplates with different geometries and plate theories [28,29]. It is worth commenting that functionally graded material (FGM) is a class of composite material which often consists of two different constituents varying their properties smoothly from one surface to another. Furthermore, the FG body can be deliberately tailored to inherit advantageous mechanical and thermal properties from the constituents of which it is made. A ceramic-metal FGM, for instance, benefits from the higher thermal resistance and better ductility from ceramic and metal phases, respectively. In addition, FGMs avoid stress concentration and delamination phenomena which are severe drawbacks of lightweight laminated composites. These striking features enable this material to be widely applied in various engineering fields such as aerospace, nuclear power plant, and bio-engineering in which the high-performance beam [30,31], plate [32,33] and shell [34] elements are involved.

When attention is turned to plate structures, there is a well established body of work on the development of mathematical models. The most basic plate theory is the classical plate theory (CPT), also known as Kirchhoff-Love plate theory. This theory basically assumes that the cross section perpendicular to the mid-plane before deformation remains normal to the mid-plane after deformation. As CPT neglects shear deformations, it is applicable only for thin plates in which the ratios of length to thickness are large. The first-order shear deformation theory (FSDT), also known as Reissner-Mindlin plate theory, was developed taking into account the shear deformations. This advantageous feature enables FSDT to yield reliable results for both thin and thick plates. However, the shear locking phenomenon which creates higher stiffness is often cited as a drawback of this theory when the problems are solved numerically by means of lower-order FEM. In addition, FSDT fails to predict the distribution of shear strains and stresses through the thickness for structures with traction free surfaces. In order to address this issue, one may need to include shear cor-

rection factor while using FSDT. However, this is not a straightforward approach as the shear correction factor does not stay the same for different problems. In order to bypass those shortcomings, Reddy pioneered the third-order shear deformation theory (TSDT) [35] before Soldatos proposed the higher-order shear deformation theory (HSDT) [36]. By making further assumptions to the TSDT, Senthilnathan [37] developed refined plate theory (RPT) which requires only four variables compared to Reddy's original five-unknown theory. In the last few years, the studies of the behaviours of microplates employing MCST and different plate theories have been enriched with a wealth of numerical solutions and analytical approaches. Reddy and his colleagues have successfully developed finite element models to analyse the behaviours of microplates with and without nonlinearity [28,38,39]. Similarly, Zhang et al. [40] presented the bending, free vibration, and buckling analyses with MCST by means of C^0 finite element method. Concerning the analytical approaches, Thai and his colleagues [27,41] investigated the bending and vibration responses of the FG microplates based on the TSDT and sinusoidal plate models with MCST. A size-dependent refined plate model for FG microplates based on MCST have been employed to solve for the closed-form solutions by He et al. [42]. It should be noted that although the RPT which requires only four unknowns owns positive properties compared to other models, it requires C^1 -continuity elements which may cause difficulty when the conventional FEA is involved to solve the problem.

Recently, a newly developed numerical method which is able to deal with higher-order elements was initially coined Isogeometric Analysis by Hughes et al. [43]. This method also bridges the crucial gaps between the computer-aided design (CAD) field and the analysis field as it employs the same basis functions for representing geometries and conducting analysis. With well established works on CAD technology, the basis functions which commonly are B-splines or Non-Uniform Rational B-splines (NURBS) are able to exactly represent geometries. Furthermore, by its nature, those functions are highly smooth and can serve as the approximation basis of the unknowns. Also, when combined with appropriate plate theory, IGA is able to avoid locking phenomena as well as other techniques such as strain smoothing [44]. These positive properties make the IGA outweighs traditional FEA in many cases, especially for numerical problems where the high-continuity elements are involved such as C^1 plate analysis using HSDT or RPT. The basics and review of IGA as well as its computer implementation could be found in the established literature including the excellent works of Cottrell et al. [45], Vuong et al. [46], de Falco et al. [47], and Nguyen et al. [48]. IGA is also widely applied to solve for mechanical and thermal behaviours of complex structures such as plates [49–52] and shells [53–56]. Although IGA-based nonlinear analysis for plates has been touched following the works of the researchers in the community including [57–59], there is no reports on the nonlinear analysis of small-scale plates for size-dependent effects using this robust numerical method.

In this study, in order to fill the existing gap in the literature, the nonlinear analysis of FG microplates by means of the IGA will be proposed. The MCST with only one material length scale parameter is employed to account for the size-dependent effects of the small-scale FG plates. Meanwhile, the four-unknown RPT is used to describe the generalised displacement field of the microplates. The bending responses with nonlinearity are then numerically solved by the proposed NURBS-based IGA in which the iterative Newton-Raphson algorithm is involved. It is worth commenting that although there is still room for the performance of the NURBS functions regarding geometry representation as the domains of the plates considered in this study are not of high

complexity, NURBS-based IGA is significantly advantageous compared to the tradition FEA in dealing with high-continuity elements which is essentially required in the proposed studies with C^1 RPT and MCST involved.

The outline of this study is as follows. The next section presents a brief review on the derivation of the MCST accounting for the size-dependent effects. The kinematics of the FG microplates and proposed RPT with nonlinearity are included in Section 3. Section 4 details the IGA basis functions and NURBS-based formulation for microplates as well as the Newton-Raphson iterative procedure which is employed to solve the nonlinear problems. Section 5 presents numerical examples containing convergence and verification studies as well as nonlinear bending analyses of square and circle microplates. The study is closed with concluding remarks which are given in Section 6.

2. Review of the modified couple stress theory

As an expansion to the classical elasticity, the MCST includes both the classical terms and the couple stress terms in the structural strain energy which can be expressed as

$$U = \int_V (\boldsymbol{\sigma} : \boldsymbol{\varepsilon} + \mathbf{m} : \boldsymbol{\chi}) dV, \quad (1)$$

where the first two components correspond to the classical terms with the Cauchy stress tensor $\boldsymbol{\sigma}$ and the strain tensor $\boldsymbol{\varepsilon}$, while the last two components represent couple stress terms which include the deviatoric part of the couple stress tensor \mathbf{m} and symmetric curvature tensor $\boldsymbol{\chi}$. The strain tensor $\boldsymbol{\varepsilon}$ and the symmetric curvature tensor $\boldsymbol{\chi}$ are defined via the relation with the displacement vector \mathbf{u} and the rotation vector $\boldsymbol{\theta}$ as follows

$$\boldsymbol{\varepsilon} = \frac{1}{2} [\nabla \mathbf{u} + (\nabla \mathbf{u})^T], \quad (2a)$$

$$\boldsymbol{\chi} = \frac{1}{2} [\nabla \boldsymbol{\theta} + (\nabla \boldsymbol{\theta})^T], \quad (2b)$$

in which the rotation vector $\boldsymbol{\theta}$ is also geometrically derived from the displacement vector \mathbf{u} as

$$\boldsymbol{\theta} = \frac{1}{2} \text{curl}(\mathbf{u}). \quad (3)$$

Having those classical and couple stress terms defined, the constitutive equations are assumed to be of the form

$$\boldsymbol{\sigma} = \lambda \text{tr}(\boldsymbol{\varepsilon}) \mathbf{I} + 2\mu \boldsymbol{\varepsilon}, \quad (4a)$$

$$\mathbf{m} = 2\mu \ell^2 \boldsymbol{\chi}, \quad (4b)$$

where ℓ is the material length scale parameter measuring the effect of couple stress, \mathbf{I} denotes the identity matrix, and $\text{tr}(\boldsymbol{\varepsilon})$ is the trace of the strain tensor (ε_{kk}). Meanwhile, λ and μ (which is also widely known as shear modulus G) are the classical elasticity's Lamé's constants calculated by

$$\lambda = \frac{\nu E}{(1+\nu)(1-2\nu)}, \quad (5a)$$

$$\mu = \frac{E}{2(1+\nu)}, \quad (5b)$$

where E and ν are the Young's modulus and Poisson's ratio, respectively.

It is worth commenting that the material length scale parameter ℓ explicitly depends on the material and its specific value can be experimentally determined from either bending tests of thin beams [1] or torsional experiments of slender cylinders [60]. According to Mindlin [6], the material length scale can be esti-

ated theoretically by taking the square root of the ratio of curvature modulus to shear modulus.

3. Kinematics of FG microplates

3.1. Functionally graded materials

The FGMs which are typically made of ceramic and metal can be homogeneously modelled following either the rule of mixtures (Voigt scheme) [61] or the Mori-Tanaka scheme [62]. Those models assume FGMs to be homogeneous materials with the equivalent effective properties which are calculated from the properties of both, ceramic and metal constituents, depending on their proportions. For the material models, the volume fractions of ceramic phase V_c and metal phase V_m through the structure's thickness h are described by

$$V_c(z) = \left(\frac{1}{2} + \frac{z}{h}\right)^n, \quad V_m = 1 - V_c, \quad -\frac{h}{2} \leq z \leq \frac{h}{2}, \quad (6)$$

where n is the material index which indicates the profile of material variation through the thickness. It is worth commenting that $n = 0$ implies a fully homogeneous ceramic material, and the material properties tend to the fully homogeneous metal as n increases towards $+\infty$. The above equation of volume fractions also implies a smooth variation of the material from the bottom surface with metal to the top surface with ceramic.

The effective properties of FGM, according to the rule of mixtures, are calculated as follows

$$E_e = E_m V_m + E_c V_c, \quad (7a)$$

$$\nu_e = \nu_m V_m + \nu_c V_c, \quad (7b)$$

where E and ν represent the elastic Young's modulus and Poisson's ratio of metal phase (subscript m) and ceramic phase (subscript c), respectively. In spite of the simplicity and ease of implementation, the rule of mixtures model fails to describe the interactions between the constituents. Therefore the Mori-Tanaka scheme was developed taking those interactions into account. This model introduces the effective bulk modulus K_e and the shear modulus G_e which are expressed as

$$\frac{K_e - K_m}{K_c - K_m} = \frac{V_c}{1 + V_m \frac{K_c - K_m}{K_m + \frac{4}{3} G_m}}, \quad \frac{G_e - G_m}{G_c - G_m} = \frac{V_c}{1 + V_m \frac{G_c - G_m}{G_m + f_1}}, \quad (8)$$

where

$$f_1 = \frac{G_m(9K_m + 8G_m)}{6(K_m + 2G_m)}. \quad (9)$$

The effective Young's modulus and Poisson's ratio are then calculated as

$$E_e = \frac{9K_e G_e}{3K_e + G_e}, \quad \nu_e = \frac{3K_e - 2G_e}{2(3K_e + G_e)}. \quad (10)$$

The variations of the former according the two material models are illustrated in Fig. 1. It can be seen that although there are differences between the rule of mixtures and Mori-Tanaka scheme, the effective properties including Young's modulus vary smoothly from the bottom surface to the top surface reflecting what expected previously.

3.2. Nonlinear refined plate theory

According to the RPT which is initially proposed by Senthilnathan et al. [37] after making further assumptions to the third-order shear deformation model of Reddy [35], the plates'

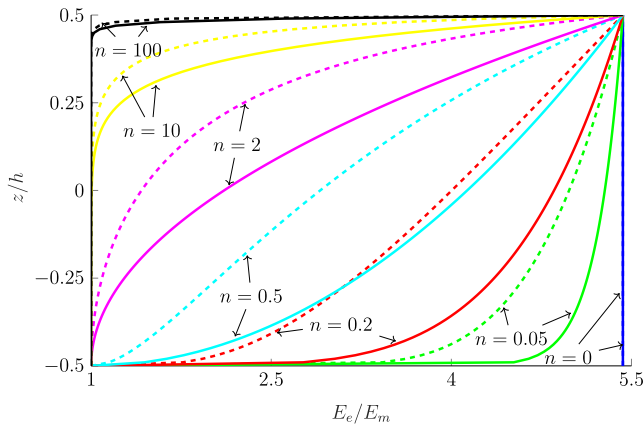
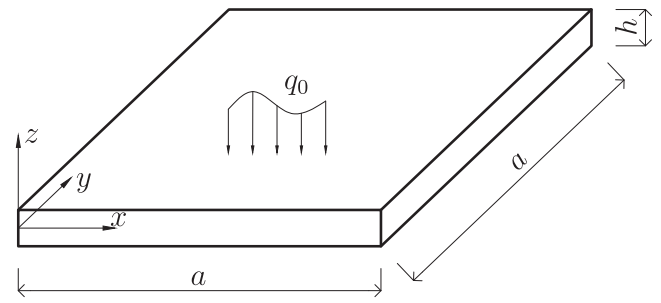
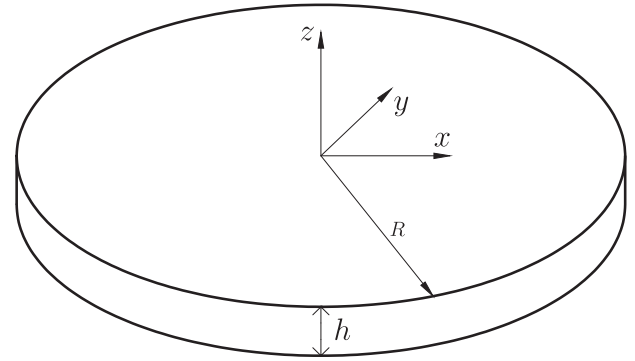


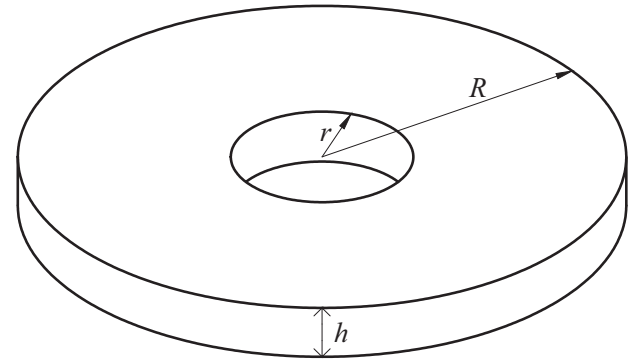
Fig. 1. The effective modulus of Al/Al₂O₃ plates according to the rule of mixtures (in solid lines) and Mori-Tanaka scheme (in dash lines).



(a) Square plate



(b) Circular plate



(c) Annular plate

Fig. 3. Geometric configurations.

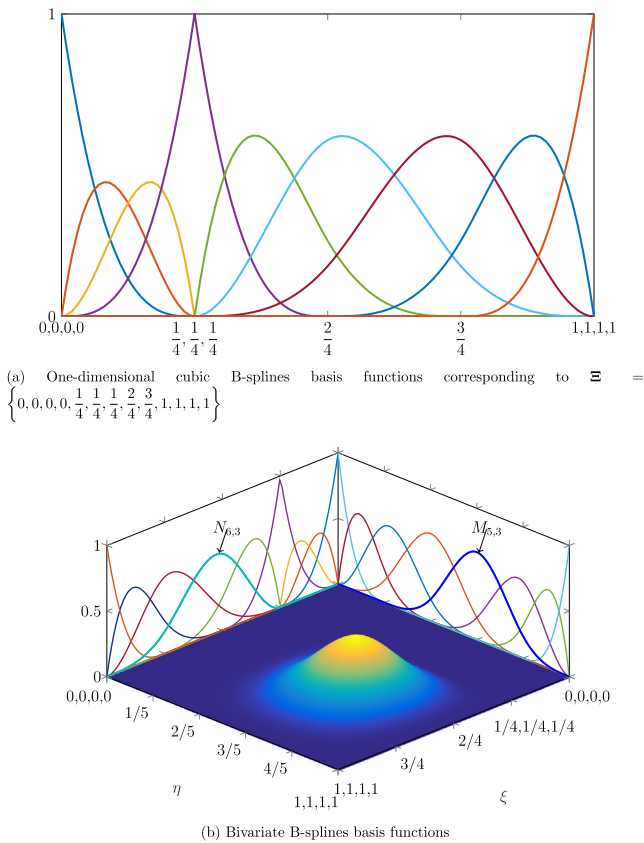


Fig. 2. One- and two-dimensional B-splines basis functions.

Table 1
Material properties.

Material	Type	E_c (ceramic)	E_m (metal)	ν_1	ν_2
Material I [66]	Isotropic	3×10^7 psi	3×10^7 psi	0.316	0.316
Material II [29]	FGM	14.4 GPa	1.44 GPa	0.3	0.3
Material III [28]	FGM	1.0×10^6	1.0×10^5	0.25	0.25
Al/Al ₂ O ₃	FGM	380 GPa	70 GPa	0.3	0.3
Al/ZnO ₂	FGM	151 GPa	70 GPa	0.3	0.3
Al/SiC	FGM	427 GPa	70 GPa	0.17	0.3

displacement field, for $z \in [-\frac{h}{2}, \frac{h}{2}]$, with only four unknowns can be expressed as

$$u(x, y, z) = u_0(x, y) - zW_{b,x}(x, y) + g(z)w_{s,x}(x, y), \tag{11a}$$

$$v(x, y, z) = v_0(x, y) - zW_{b,y}(x, y) + g(z)w_{s,y}(x, y), \tag{11b}$$

$$w(x, y, z) = w_b(x, y) + w_s(x, y), \tag{11c}$$

where u_0 and v_0 are displacement components of a material point at $(x, y, 0)$ in x and y coordinate directions, respectively. While w_b and w_s represent the bending and shear components of transverse displacement, respectively, the function g is introduced to describe the distribution of transverse strains and stresses through the thickness, $g : z \mapsto g(z) = f(z) - z$. It should be noted that, in order to have the traction-free conditions satisfied at the top and bottom surfaces, the first derivative of f should be zero at $z = \pm h/2$. In this study, the polynomial function f which is proposed by Nguyen et al. [63] will be used.

The general nonlinear strains can be derived from the displacement fields as

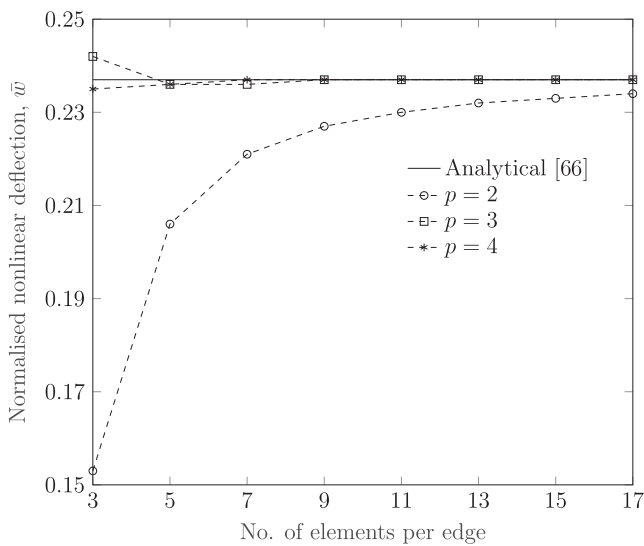


Fig. 4. Convergence of nonlinear central deflection of fully clamped isotropic plates with different meshes and polynomial orders, $a/h = 100, a = 300 \text{ in.}, h = 3 \text{ in.}, P = 17.79$ (Material I).

Table 2

Comparison of normalised nonlinear deflection $\bar{w}(\frac{a}{2}, \frac{a}{2}, 0)$ and normal stress $\bar{\sigma}_x(\frac{a}{2}, \frac{a}{2}, \frac{h}{2})$ of clamped isotropic square plates under uniform loading (Material I), $a/h = 100$.

P	Response	Nonlinear						Linear	
		Present	Analytical [66]	FEM [67]	C ⁰ -FEM [68]	MXFEM [69]	IGA FSDT [57]	Present	MXFEM [69]
17.79	\bar{w}	0.2365	0.237	0.2368	0.2385	0.2392	0.2328	0.2435	0.2465
	$\bar{\sigma}_x$	2.5602	2.6	2.6319	2.6733	2.414	-	2.4643	2.387
38.3	\bar{w}	0.4692	0.471	0.4699	0.4725	0.4738	0.4635	0.5243	0.5307
	$\bar{\sigma}_x$	5.3256	5.2	5.4816	5.5733	5.022	-	5.3054	5.138
63.4	\bar{w}	0.6908	0.695	0.6915	0.6948	0.6965	0.6854	0.8678	0.8785
	$\bar{\sigma}_x$	8.0973	8.0	8.3258	8.4867	7.649	-	8.7822	8.510
95.0	\bar{w}	0.9024	0.912	0.9029	0.9065	0.9087	0.8985	1.3004	1.3163
	$\bar{\sigma}_x$	10.8248	11.1	11.103	11.3500	10.254	-	13.1595	12.745
134.9	\bar{w}	1.1060	1.121	1.1063	1.1100	1.1130	1.1045	1.8466	1.8692
	$\bar{\sigma}_x$	13.5187	13.3	13.827	14.1700	12.850	-	18.6865	18.099
184.0	\bar{w}	1.3008	1.323	1.3009	1.3046	1.3080	1.3020	2.5187	2.5495
	$\bar{\sigma}_x$	16.1771	15.9	16.497	16.9367	15.420	-	25.4879	24.686
245.0	\bar{w}	1.4926	1.521	1.4928	1.4963	1.5010	1.4969	3.3536	3.3947
	$\bar{\sigma}_x$	18.9019	19.2	19.225	19.7633	18.060	-	33.9377	32.869
318.0	\bar{w}	1.6784	1.714	1.6786	1.6820	1.6880	1.6856	4.3529	4.4062
	$\bar{\sigma}_x$	21.6744	21.9	21.994	22.6367	20.741	-	44.0498	42.664
402.0	\bar{w}	1.8552	1.902	1.8555	1.8590	1.8660	1.8652	5.5027	5.5702
	$\bar{\sigma}_x$	24.4624	25.1	24.780	25.5367	23.423	-	55.6855	53.933

$$\varepsilon_{ij} = \frac{1}{2}(u_{i,j} + u_{j,i}) + \frac{1}{2}u_{k,i}u_{k,j}. \tag{12}$$

If the small strain assumptions are applied, the components of the displacement gradients are neglected. Meanwhile, assuming that the rotations of the transverse normals are moderate, the terms of derivatives of transverse displacement, $(w_x)^2, (w_y)^2, w_x w_y$, are small but not negligible [64]. In such case, small strains and moderate rotations, the displacement-strain relations associated with the RPT with the von Kármán strains can be expressed as follows

$$\boldsymbol{\varepsilon} = \boldsymbol{\varepsilon}_0 + z\boldsymbol{\kappa}_b + g(z)\boldsymbol{\kappa}_s, \tag{13a}$$

$$\boldsymbol{\gamma} = [1 + g'(z)]\boldsymbol{\varepsilon}_s = f'(z)\boldsymbol{\varepsilon}_s, \tag{13b}$$

where

$$\boldsymbol{\varepsilon} = [\varepsilon_x \quad \varepsilon_y \quad \gamma_{xy}]^T, \tag{14a}$$

$$\boldsymbol{\gamma} = [\gamma_{xz} \quad \gamma_{yz}]^T, \tag{14b}$$

and the in-plane, bending and shear strains are expressed as

$$\boldsymbol{\varepsilon}_0 = \boldsymbol{\varepsilon}_0^L + \boldsymbol{\varepsilon}_0^{NL}, \quad \boldsymbol{\kappa}_b = - \begin{bmatrix} w_{b,xx} \\ w_{b,yy} \\ 2w_{b,xy} \end{bmatrix}, \quad \boldsymbol{\kappa}_s = \begin{bmatrix} w_{s,xx} \\ w_{s,yy} \\ 2w_{s,xy} \end{bmatrix}, \quad \boldsymbol{\varepsilon}_s = \begin{bmatrix} w_{s,x} \\ w_{s,y} \end{bmatrix} \tag{15}$$

with the linear and nonlinear components of the in-plane strains are defined as

$$\boldsymbol{\varepsilon}_0^L = \begin{bmatrix} u_{0,x} \\ v_{0,y} \\ u_{0,y} + v_{0,x} \end{bmatrix}, \quad \boldsymbol{\varepsilon}_0^{NL} = \frac{1}{2}\mathbf{A}_\vartheta \boldsymbol{\vartheta}, \tag{16}$$

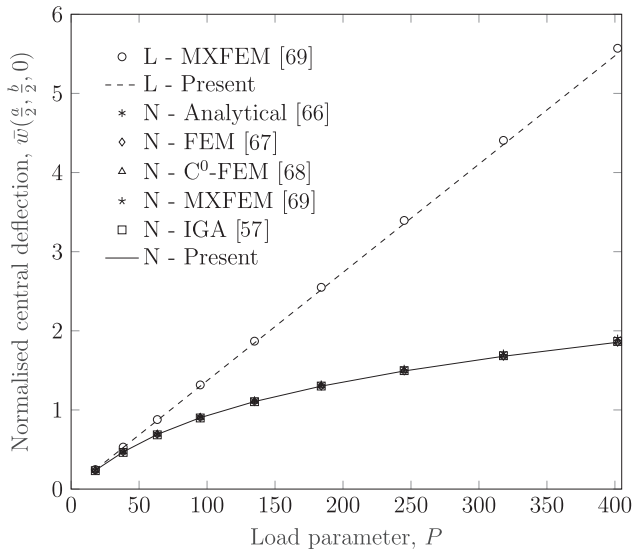
where

$$\mathbf{A}_\vartheta = \begin{bmatrix} w_{b,x} + w_{s,x} & 0 \\ 0 & w_{b,y} + w_{s,y} \\ w_{b,y} + w_{s,y} & w_{b,x} + w_{s,x} \end{bmatrix}, \quad \boldsymbol{\vartheta} = \begin{bmatrix} w_{b,x} + w_{s,x} \\ w_{b,y} + w_{s,y} \end{bmatrix}. \tag{17}$$

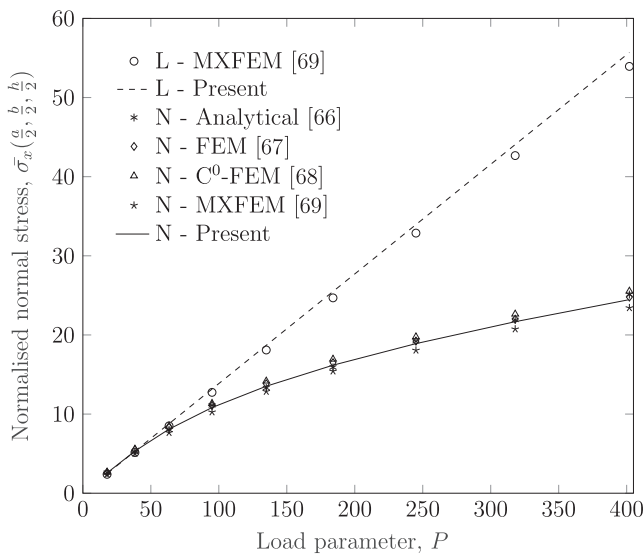
By using Eqs. (2b), (3) and (11), the couple stress terms of rotation vector and curvature tensor can be obtained as follows

$$\boldsymbol{\theta} = \begin{bmatrix} \theta_1 \\ \theta_2 \\ \theta_3 \end{bmatrix} = \frac{1}{2} \begin{bmatrix} 2w_{b,y} - (g' - 1)w_{s,y} \\ -2w_{b,x} + (g' - 1)w_{s,x} \\ v_{0,x} - u_{0,y} \end{bmatrix}, \tag{18a}$$

$$\boldsymbol{\chi} = \begin{bmatrix} \chi_b \\ \chi_s \end{bmatrix} = \begin{bmatrix} \chi_{b0} \\ \chi_{s0} \end{bmatrix} + \begin{bmatrix} g' \chi_{b1} \\ g'' \chi_{s2} \end{bmatrix}, \tag{18b}$$



(a) Central deflection



(b) Normal stress

Fig. 5. Comparison of nonlinear (a) central deflection and (b) normal stress of fully-clamped isotropic square plates (Material I) with existing results. Prefixes L and N denote linear and nonlinear solutions, respectively.

where

$$\chi_b = \begin{bmatrix} \chi_{11} \\ \chi_{22} \\ \chi_{12} \end{bmatrix}, \quad \chi_s = \begin{bmatrix} \chi_{13} \\ \chi_{23} \end{bmatrix}, \quad (19a)$$

$$\chi_{b0} = \frac{1}{4} \begin{bmatrix} 4w_{b,xy} + 2w_{s,xy} \\ -4w_{b,xy} - 2w_{s,xy} \\ 2(-w_{b,xx} + w_{b,yy}) + (-w_{s,xx} + w_{s,yy}) \end{bmatrix}, \quad \chi_{b1} = \frac{1}{4} \begin{bmatrix} -2w_{s,xy} \\ 2w_{s,xy} \\ w_{s,xx} - w_{s,yy} \end{bmatrix}, \quad (19b)$$

$$\chi_{s0} = \frac{1}{4} \begin{bmatrix} -u_{0,xy} + v_{0,xx} \\ -u_{0,yy} + v_{0,xy} \end{bmatrix}, \quad \chi_{s2} = \frac{1}{4} \begin{bmatrix} -w_{s,y} \\ w_{s,x} \end{bmatrix}. \quad (19c)$$

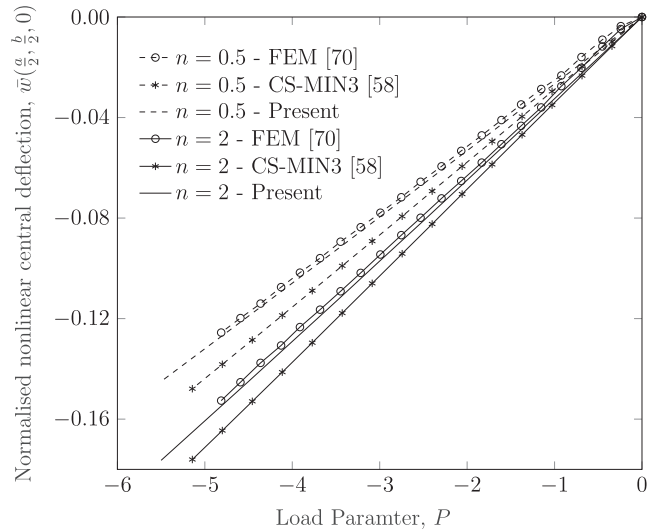


Fig. 6. Comparison of nonlinear central deflection of SSSS square Al/ZnO₂ with uniformly distributed load, $a = 0.2$ m, $h = 0.01$ m (rule of mixtures scheme).

It is worth commenting that in this particular case using the displacement field in Eq. (11), the curvature component of χ_{33} is identically zero. Having the strain terms and the curvature tensor derived, the classical and modified couple stress constitutive relations of FG microplates can be obtained as follows

$$\begin{Bmatrix} \sigma_x \\ \sigma_y \\ \sigma_{xy} \\ \tau_{xz} \\ \tau_{yz} \end{Bmatrix} = \begin{bmatrix} Q_{11} & Q_{12} & 0 & 0 & 0 \\ Q_{21} & Q_{22} & 0 & 0 & 0 \\ 0 & 0 & Q_{66} & 0 & 0 \\ 0 & 0 & 0 & Q_{55} & 0 \\ 0 & 0 & 0 & 0 & Q_{44} \end{bmatrix} \begin{Bmatrix} \epsilon_x \\ \epsilon_y \\ \epsilon_{xy} \\ \gamma_{xz} \\ \gamma_{yz} \end{Bmatrix}, \quad (20a)$$

$$\begin{Bmatrix} m_{11} \\ m_{22} \\ m_{33} \\ m_{12} \\ m_{13} \\ m_{23} \end{Bmatrix} = \begin{bmatrix} 2G_e \ell^2 & 0 & 0 & 0 & 0 & 0 \\ 0 & 2G_e \ell^2 & 0 & 0 & 0 & 0 \\ 0 & 0 & 2G_e \ell^2 & 0 & 0 & 0 \\ 0 & 0 & 0 & 2G_e \ell^2 & 0 & 0 \\ 0 & 0 & 0 & 0 & 2G_e \ell^2 & 0 \\ 0 & 0 & 0 & 0 & 0 & 2G_e \ell^2 \end{bmatrix} \begin{Bmatrix} \chi_{11} \\ \chi_{22} \\ \chi_{33} \\ \chi_{12} \\ \chi_{13} \\ \chi_{23} \end{Bmatrix}, \quad (20b)$$

where

$$Q_{11} = Q_{22} = \frac{E_e(z)}{1 - (v_e(z))^2}, \quad Q_{12} = Q_{21} = \frac{E_e(z)v_e(z)}{1 - (v_e(z))^2}, \quad (21a)$$

$$Q_{44} = Q_{55} = Q_{66} = \frac{E_e(z)}{2(1 + v_e(z))}, \quad (21b)$$

$$G_e = \frac{E_e(z)}{2(1 + v_e(z))}.$$

Meanwhile, the classical stress resultants are calculated as

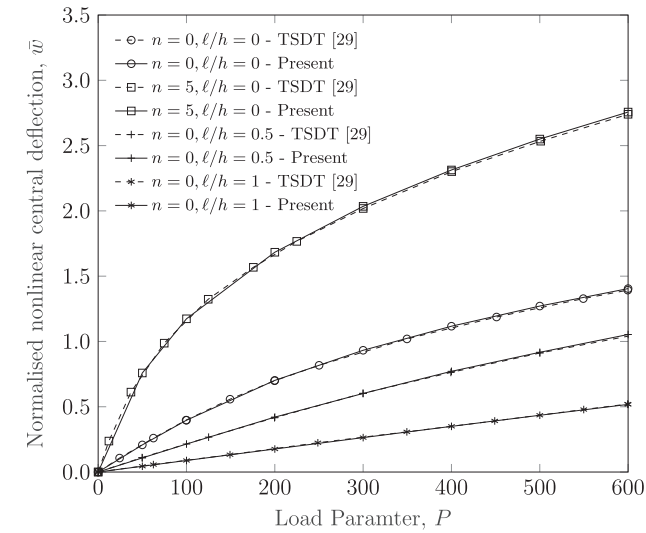
$$\begin{bmatrix} \mathbf{N} \\ \mathbf{M}^b \\ \mathbf{M}^s \end{bmatrix} = \mathbf{D}^b \boldsymbol{\epsilon}_b, \quad (22a)$$

$$\mathbf{Q} = \mathbf{D}^s \boldsymbol{\epsilon}_s, \quad (22b)$$

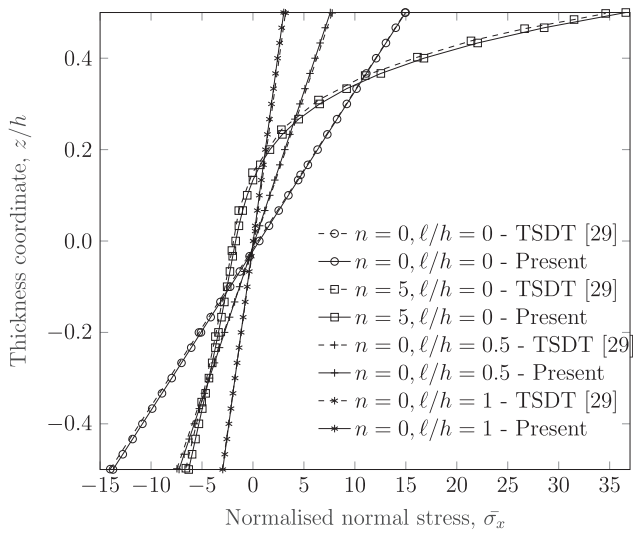
where

Table 3
Degrees of freedom required in FEM and IGA approaches.

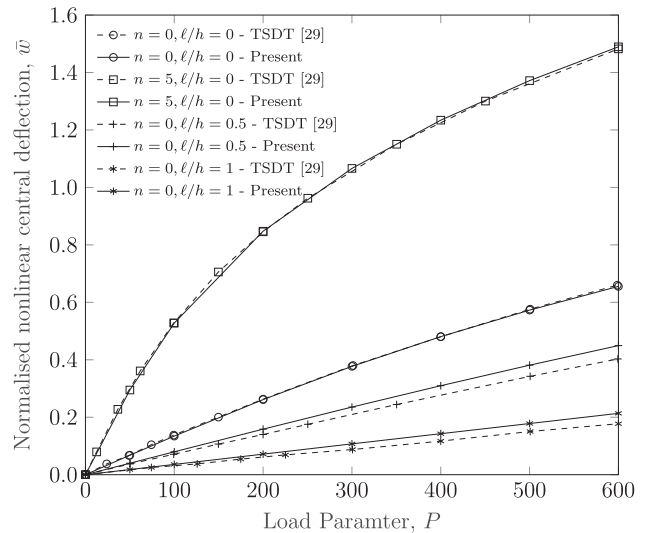
Approach	# Unknowns	Element type	Mesh	Total DOFs
FEM and GTPT [29]	11	Cubic	16 × 16	12716
IGA and RPT (present)	4	Cubic	11 × 11	784



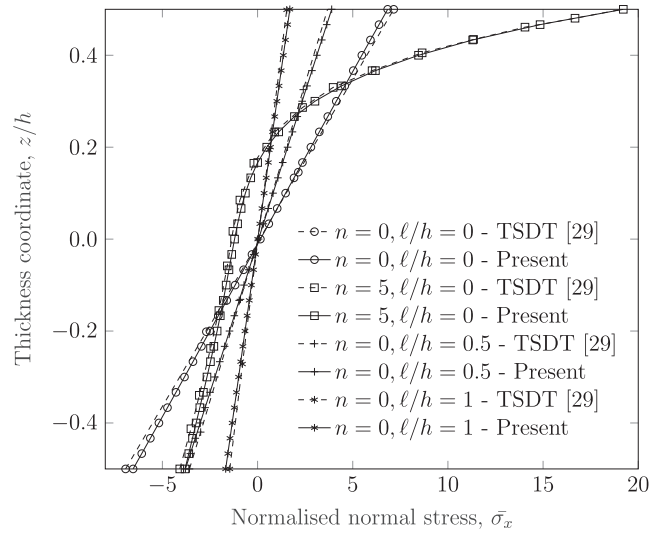
(a) Central deflection $\bar{w}(\frac{a}{2}, \frac{b}{2}, 0)$



(b) Normal stress $\bar{\sigma}_x(\frac{9a}{16}, \frac{9a}{16}, z), P = 50$



(a) Central deflection $\bar{w}(\frac{a}{2}, \frac{b}{2}, 0)$



(b) Normal stress $\bar{\sigma}_x(\frac{9a}{16}, \frac{9a}{16}, z), P = 50$

Fig. 7. Comparison of nonlinear (a) central deflection and (b) normal stress of SSSS FG square microplates, $a/h = 20$, rule of mixtures scheme (Material I).

Fig. 8. Comparison of nonlinear (a) central deflection and (b) normal stress of CCCC FG square microplates, $a/h = 20$, rule of mixtures scheme (Material II).

$$\mathbf{N} = \begin{bmatrix} N_x \\ N_y \\ N_{xy} \end{bmatrix}, \quad \mathbf{M}^b = \begin{bmatrix} M_x^b \\ M_y^b \\ M_{xy}^b \end{bmatrix}, \quad \mathbf{M}^s = \begin{bmatrix} M_x^s \\ M_y^s \\ M_{xy}^s \end{bmatrix}, \quad \mathbf{Q} = \begin{bmatrix} Q_{xz} \\ Q_{yz} \end{bmatrix}, \quad (23a)$$

$$\boldsymbol{\varepsilon}_b = \begin{bmatrix} \varepsilon_0 \\ \boldsymbol{\kappa}_b \\ \boldsymbol{\kappa}_s \end{bmatrix}, \quad \mathbf{D}^b = \begin{bmatrix} \mathbf{A} & \mathbf{B} & \mathbf{E} \\ \mathbf{B} & \mathbf{D} & \mathbf{F} \\ \mathbf{E} & \mathbf{F} & \mathbf{H} \end{bmatrix}, \quad \mathbf{D}^s = \begin{bmatrix} D_{44}^s & 0 \\ 0 & D_{55}^s \end{bmatrix}, \quad (23b)$$

and the components of the material matrices are defined as follows

$$(\mathbf{A}_{ij}, \mathbf{B}_{ij}, \mathbf{D}_{ij}, \mathbf{E}_{ij}, \mathbf{F}_{ij}, \mathbf{H}_{ij}) = \int_{-h/2}^{h/2} [1, z, z^2, g(z), zg(z), g^2(z)] \hat{\mathbf{Q}}_{ij} dz, \quad (24a)$$

$$D_{ij}^s = \int_{-h/2}^{h/2} [1 + g'(z)]^2 \hat{\mathbf{Q}}_{ij} dz, \quad (24b)$$

$$\hat{\mathbf{Q}} = \begin{bmatrix} Q_{11} & Q_{12} & 0 \\ Q_{21} & Q_{22} & 0 \\ 0 & 0 & Q_{66} \end{bmatrix}, \quad (24c)$$

$$\hat{\mathbf{Q}} = \begin{bmatrix} Q_{44} & 0 \\ 0 & Q_{55} \end{bmatrix}. \quad (24d)$$

Similarly, the couple stress components are defined by

$$\begin{Bmatrix} \mathbf{N}^c \\ \mathbf{R}^c \end{Bmatrix} = \mathbf{D}_c^b \boldsymbol{\chi}_b^c, \tag{25a}$$

$$\begin{Bmatrix} \mathbf{P}^c \\ \mathbf{T}^c \end{Bmatrix} = \mathbf{D}_c^s \boldsymbol{\chi}_s^c, \tag{25b}$$

where

$$\boldsymbol{\chi}_b^c = \begin{bmatrix} \chi_{b0}^c \\ \chi_{b1}^c \end{bmatrix}, \quad \boldsymbol{\chi}_s^c = \begin{bmatrix} \chi_{s0}^c \\ \chi_{s2}^c \end{bmatrix}, \quad \mathbf{D}_c^b = \begin{bmatrix} \mathbf{A}^c & \mathbf{B}^c \\ \mathbf{B}^c & \mathbf{D}^c \end{bmatrix}, \quad \mathbf{D}_c^s = \begin{bmatrix} \mathbf{X}^c & \mathbf{Y}^c \\ \mathbf{Y}^c & \mathbf{Z}^c \end{bmatrix}, \tag{26}$$

and the components of the material matrices are calculated as

$$(A_{ij}^c, B_{ij}^c, D_{ij}^c) = \int_{-h/2}^{h/2} (1, g'(z), [g'(z)]^2) \bar{G}_{ij} dz, \tag{27a}$$

$$(X_{ij}^c, Y_{ij}^c, Z_{ij}^c) = \int_{-h/2}^{h/2} (1, g''(z), [g''(z)]^2) \hat{G}_{ij} dz, \tag{27b}$$

$$\bar{\mathbf{G}} = 2G_e \ell^2 \begin{bmatrix} 1 & 0 & 0 \\ 0 & 1 & 0 \\ 0 & 0 & 1 \end{bmatrix}, \tag{27c}$$

$$\hat{\mathbf{G}} = 2G_e \ell^2 \begin{bmatrix} 1 & 0 \\ 0 & 1 \end{bmatrix}. \tag{27d}$$

After applying the derivation of the Hamilton's principal and weak formulation, the weak form of the nonlinear bending problem of FG microplates subjected to transverse load q_0 can be briefly expressed as [63]

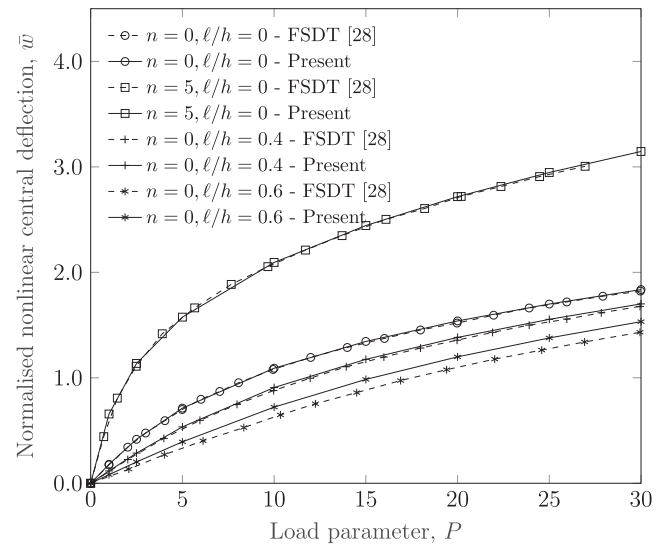
$$\int_{\Omega} \delta \boldsymbol{\varepsilon}_b^T \mathbf{D}_c^b \boldsymbol{\varepsilon}_b d\Omega + \int_{\Omega} \delta \boldsymbol{\varepsilon}_s^T \mathbf{D}_c^s \boldsymbol{\varepsilon}_s d\Omega + \int_{\Omega} (\delta \boldsymbol{\chi}_b^c)^T \mathbf{D}_c^b \boldsymbol{\chi}_b^c d\Omega + \int_{\Omega} (\delta \boldsymbol{\chi}_s^c)^T \mathbf{D}_c^s \boldsymbol{\chi}_s^c d\Omega = \int_{\Omega} \delta w q_0 d\Omega. \tag{28}$$

4. NURBS-based approach for nonlinear analysis of FG microplates

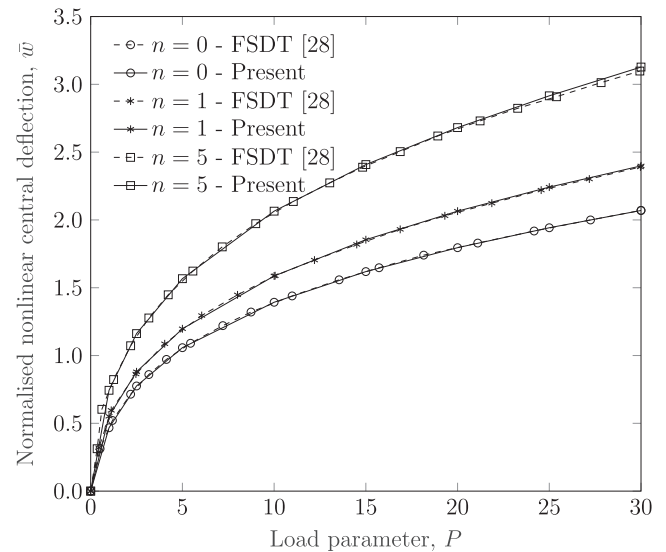
This section details the basis functions including B-splines and Non-Uniform Rational B-splines (NURBS) which are used for the isogeometric analysis. In addition, the NURBS-based formulation of microplates with MCST will also be addressed. This formulation is derived in the accordance with the kinematics of FG microplates which has been presented in Section 3. Furthermore, this section also includes the description of the Newton-Raphson iterative procedure which is employed to solve the proposed nonlinear problems of FG microplates by means of isogeometric analysis.

4.1. B-splines and NURBS basis functions

The primary point of the B-splines is a knot vector which is a set of non-decreased coordinates in the parameter space, $\boldsymbol{\Xi} = \{\xi_1, \xi_2, \dots, \xi_{n+p+1}\}$, where i is the knot index of the i^{th} knot $\xi_i \in R$, n is the number of basis functions and p represents the polynomial order of the basis function. A knot vector is called uniform if its knots are equally spaced while it is open if the first knot and the last knot are simultaneously repeated $p + 1$ times. It is worth noting that even though 1-D basis functions with open knot vectors are interpolatory at the two ends of the space interval, ξ_1 and ξ_{n+p+1} , they are generally not interpolatory at the remaining knots, i.e. interior knots. This property distinguishes the features of the knots from the nodes in the FEA.



(a) Clamped plates



(b) Simply-supported plates, $\ell/h = 0.6$

Fig. 9. Comparison of nonlinear central deflection of FG circular microplates subjected to uniformly distributed load, $R = 1, h = 0.1$, rule of mixtures scheme (Material III), $P = \frac{q_0 R^4}{E_c h^4}$.

According to the Cox-de Boor recursion algorithm, the B-spline basis functions of order p are defined recursively, starting with the piecewise constant ($p = 0$), as follow

$$N_{i,0}(\xi) = \begin{cases} 1 & \text{if } \xi_i \leq \xi < \xi_{i+1}, \\ 0 & \text{otherwise.} \end{cases} \tag{29}$$

Subsequently, the basis functions for higher order ($p \geq 1$) are constructed as

$$N_{i,p}(\xi) = \frac{\xi - \xi_i}{\xi_{i+p} - \xi_i} N_{i,p-1}(\xi) + \frac{\xi_{i+p+1} - \xi}{\xi_{i+p+1} - \xi_{i+1}} N_{i+1,p-1}(\xi). \tag{30}$$

The B-splines basis functions, by their nature, are piecewise non-negative. In addition, while the functions are C^∞ continuous inside knot spans, they are C^{p-k} continuous across the knots, where k is the multiplicity of the knot. This property enables the continuity of the basis function to be tailored with flexibility by adjusting either polynomial order p or the knot multiplicity k .

Table 4
Normalised deflection $\bar{w}(\frac{a}{2}, \frac{a}{2}, 0)$ and normal stress $\bar{\sigma}_x(\frac{a}{2}, \frac{a}{2}, \frac{h}{2})$ of SSSS square Al/Al₂O₃ microplates (rule of mixtures scheme, $n = 1$).

a/h	ℓ/h	P = 1		P = 50		P = 100		P = 200		P = 300		P = 400	
		\bar{w}	$\bar{\sigma}_x$	\bar{w}	$\bar{\sigma}_x$	\bar{w}	$\bar{\sigma}_x$	\bar{w}	$\bar{\sigma}_x$	\bar{w}	$\bar{\sigma}_x$	\bar{w}	$\bar{\sigma}_x$
<i>Uniformly distributed load</i>													
5	0.0	0.0192	0.4585	0.7281	20.2345	1.1161	32.2415	1.6088	48.0796	1.9627	59.8543	2.2512	69.7203
	0.2	0.0158	0.3740	0.6508	17.9251	1.0342	29.9180	1.5183	45.8654	1.8577	57.5988	2.1297	67.3703
	0.4	0.0103	0.2401	0.4792	12.7399	0.8359	23.8318	1.3151	40.0759	1.6491	52.1288	1.9128	62.0664
	0.6	0.0066	0.1497	0.3208	8.1036	0.6069	16.5265	1.0555	31.4986	1.3888	43.7129	1.6541	53.9939
	0.8	0.0043	0.0977	0.2159	5.2192	0.4235	10.9089	0.7952	22.5595	1.1054	33.5254	1.3657	43.4703
	1.0	0.0030	0.0674	0.1514	3.5450	0.3006	7.3965	0.5859	15.6914	0.8470	24.2801	1.0820	32.7521
20	0.0	0.0166	0.4463	0.6703	20.6394	1.0521	33.5078	1.5222	49.6254	1.8445	60.9439	2.0996	70.1634
	0.2	0.0138	0.3690	0.5960	18.1802	0.9745	31.0510	1.4496	47.6881	1.7747	59.3446	2.0306	68.7622
	0.4	0.0092	0.2424	0.4338	12.8277	0.7774	24.4374	1.2547	41.7285	1.5882	54.2994	1.8494	64.3973
	0.6	0.0059	0.1539	0.2890	8.2205	0.5547	16.7933	0.9899	32.4265	1.3230	45.3514	1.5904	56.1730
	0.8	0.0039	0.1018	0.1945	5.3662	0.3837	11.1400	0.7317	23.0212	1.0323	34.3907	1.2901	44.8158
	1.0	0.0027	0.0709	0.1365	3.6877	0.2716	7.6322	0.5331	16.0466	0.7778	24.7742	1.0029	33.4585
<i>Sinusoidally distributed load</i>													
5	0.0	0.0123	0.3175	0.5241	15.4148	0.8496	26.3160	1.2629	41.0497	1.5527	51.8826	1.7860	60.8716
	0.2	0.0101	0.2600	0.4566	13.2402	0.7729	23.7744	1.1849	38.5672	1.4716	49.4606	1.6993	58.4438
	0.4	0.0066	0.1678	0.3201	8.9248	0.5911	17.6100	0.9908	31.8508	1.2783	42.9290	1.5055	52.1164
	0.6	0.0042	0.1050	0.2087	5.5657	0.4064	11.4858	0.7488	23.0488	1.0246	33.3911	1.2513	42.4880
	0.8	0.0028	0.0686	0.1393	3.5870	0.2763	7.4350	0.5358	15.5522	0.7699	23.7339	0.9778	31.6242
	1.0	0.0020	0.0473	0.0975	2.4465	0.1944	5.0419	0.3843	10.5897	0.5663	16.4566	0.7381	22.4713
20	0.0	0.0105	0.3057	0.4691	15.2657	0.7885	26.9596	1.1979	42.7978	1.4782	54.0753	1.6978	63.1780
	0.2	0.0087	0.2544	0.4065	13.0940	0.7125	24.2191	1.1233	40.2018	1.4071	51.7558	1.6293	61.0745
	0.4	0.0058	0.1692	0.2839	8.9138	0.5357	17.7788	0.9266	32.8919	1.2147	44.8087	1.4430	54.6267
	0.6	0.0037	0.1086	0.1856	5.6830	0.3644	11.6787	0.6853	23.5693	0.9539	34.4618	1.1796	44.1625
	0.8	0.0025	0.0723	0.1243	3.7396	0.2472	7.6921	0.4836	15.9740	0.7025	24.3722	0.9017	32.5663
	1.0	0.0017	0.0506	0.0871	2.5916	0.1739	5.3030	0.3450	11.0199	0.5110	17.0156	0.6701	23.1607

Table 5
Normalised deflection $\bar{w}(\frac{a}{2}, \frac{a}{2}, 0)$ and normal stress $\bar{\sigma}_x(\frac{a}{2}, \frac{a}{2}, \frac{h}{2})$ of CCCC square Al/Al₂O₃ microplates (rule of mixtures scheme, $n = 1$).

a/h	ℓ/h	P = 1		P = 50		P = 100		P = 200		P = 300		P = 400	
		\bar{w}	$\bar{\sigma}_x$	\bar{w}	$\bar{\sigma}_x$	\bar{w}	$\bar{\sigma}_x$	\bar{w}	$\bar{\sigma}_x$	\bar{w}	$\bar{\sigma}_x$	\bar{w}	$\bar{\sigma}_x$
<i>Uniformly distributed load</i>													
5	0.0	0.0078	0.2252	0.3489	11.8613	0.5859	21.5995	0.8826	35.6241	1.0793	46.2644	1.2298	55.2499
	0.2	0.0066	0.1894	0.3057	10.2216	0.5342	19.4510	0.8349	33.4494	1.0371	44.1720	1.1920	53.2018
	0.4	0.0045	0.1282	0.2192	7.0161	0.4116	14.3554	0.7046	27.4052	0.9158	38.1482	1.0800	47.3132
	0.6	0.0030	0.0830	0.1468	4.4753	0.2873	9.4148	0.5357	19.6087	0.7392	29.2617	0.9073	38.0758
	0.8	0.0020	0.0554	0.0999	2.9290	0.1984	6.1454	0.3864	13.1633	0.5580	20.5329	0.7118	27.8896
	1.0	0.0014	0.0387	0.0708	2.0159	0.1412	4.1914	0.2795	8.9524	0.4127	14.1324	0.5392	19.5814
20	0.0	0.0053	0.2125	0.2533	11.2046	0.4632	21.7147	0.7635	38.0455	0.9728	50.1717	1.1344	59.9860
	0.2	0.0046	0.1827	0.2234	9.6892	0.4181	19.2517	0.7128	35.1496	0.9245	47.4254	1.0892	57.4629
	0.4	0.0033	0.1286	0.1637	6.8102	0.3180	13.9886	0.5819	27.6968	0.7907	39.6071	0.9597	49.8587
	0.6	0.0023	0.0861	0.1126	4.5041	0.2230	9.3278	0.4301	19.3860	0.6139	29.3063	0.7747	38.6670
	0.8	0.0016	0.0588	0.0782	3.0404	0.1559	6.2681	0.3076	13.1496	0.4521	20.3719	0.5875	27.6997
	1.0	0.0011	0.0417	0.0561	2.1404	0.1121	4.3846	0.2230	9.1498	0.3318	14.2196	0.4376	19.5153
<i>Sinusoidally distributed load</i>													
5	0.0	0.0056	0.1796	0.2618	9.5222	0.4645	18.1651	0.7390	31.3879	0.9266	41.4695	1.0713	49.8862
	0.2	0.0047	0.1509	0.2263	8.0842	0.4150	15.9619	0.6869	28.8698	0.8776	38.9915	1.0255	47.4812
	0.4	0.0032	0.1018	0.1591	5.4485	0.3071	11.2496	0.5537	22.3444	0.7445	32.0464	0.8975	40.5132
	0.6	0.0021	0.0657	0.1056	3.4617	0.2089	7.2147	0.4013	15.1395	0.5704	23.0496	0.7171	30.5926
	0.8	0.0014	0.0436	0.0717	2.2683	0.1429	4.6983	0.2817	9.9415	0.4137	15.5190	0.5370	21.2433
	1.0	0.0010	0.0304	0.0507	1.5635	0.1013	3.2135	0.2016	6.7492	0.3000	10.5531	0.3955	14.5666
20	0.0	0.0038	0.1676	0.1861	8.7837	0.3524	17.5107	0.6129	32.4539	0.8047	44.2657	0.9556	53.9954
	0.2	0.0033	0.1445	0.1631	7.5738	0.3138	15.3170	0.5626	29.3711	0.7534	41.0311	0.9059	50.8418
	0.4	0.0024	0.1021	0.1185	5.3225	0.2332	10.9298	0.4420	22.1578	0.6195	32.6175	0.7697	42.0541
	0.6	0.0016	0.0685	0.0811	3.5377	0.1614	7.2664	0.3165	15.0797	0.4610	23.0398	0.5932	30.8616
	0.8	0.0011	0.0469	0.0562	2.4011	0.1123	4.9063	0.2230	10.1790	0.3308	15.7124	0.4346	21.4038
	1.0	0.0008	0.0334	0.0403	1.6974	0.0806	3.4511	0.1607	7.1144	0.2400	10.9624	0.3182	14.9652

Considering an additional knot vector $\mathcal{H} = \{\eta_1, \eta_2, \dots, \eta_{m+q+1}\}$ in the parametric direction of η , where m and q are the number of basis functions and the polynomial order, respectively, a 2-D B-splines basis is formed by taking tensor product of the B-splines in ξ and η directions as follow

$$N_A(\xi, \eta) = N_{i,p}(\xi)M_{j,q}(\eta) \tag{31}$$

where $M_{j,q}(\eta)$ is the j^{th} B-splines basis function of order q in η direction. The illustrations of 1-D and 2-D B-splines basis functions are presented in Fig. 2.

Table 6
Normalised deflection $\bar{w}(\frac{a}{2}, \frac{a}{2}, 0)$ and normal stress $\bar{\sigma}_x(\frac{a}{2}, \frac{a}{2}, \frac{h}{2})$ of SSSS square Al/Al₂O₃ microplates (Mori-Tanaka scheme, $n = 1$).

a/h	ℓ/h	P = 1		P = 50		P = 100		P = 200		P = 300		P = 400	
		\bar{w}	$\bar{\sigma}_x$	\bar{w}	$\bar{\sigma}_x$	\bar{w}	$\bar{\sigma}_x$	\bar{w}	$\bar{\sigma}_x$	\bar{w}	$\bar{\sigma}_x$	\bar{w}	$\bar{\sigma}_x$
<i>Uniformly distributed load</i>													
5	0.0	0.0246	0.5482	0.8626	23.2446	1.2927	36.4602	1.8441	54.2800	2.2443	67.7888	2.5677	79.1820
	0.2	0.0204	0.4508	0.7837	21.0080	1.2086	34.2580	1.7432	52.0767	2.1203	65.4499	2.4228	76.7142
	0.4	0.0134	0.2935	0.5992	15.6113	1.0078	28.4047	1.5359	46.6052	1.9021	60.1880	2.1913	71.4979
	0.6	0.0086	0.1851	0.4126	10.2260	0.7610	20.6531	1.2738	38.2544	1.6418	52.1977	1.9318	63.8747
	0.8	0.0057	0.1218	0.2807	6.6450	0.5445	13.9813	0.9944	28.6153	1.3510	41.8296	1.6419	53.5045
	1.0	0.0040	0.0845	0.1975	4.5215	0.3904	9.5413	0.7501	20.3799	1.0665	31.3703	1.3416	41.9226
20	0.0	0.0208	0.5316	0.7946	23.9070	1.2144	37.9967	1.7284	55.8226	2.0829	68.6366	2.3647	79.2409
	0.2	0.0175	0.4439	0.7194	21.4738	1.1397	35.7215	1.6590	54.0610	2.0150	67.1516	2.2964	77.9038
	0.4	0.0118	0.2965	0.5445	15.7734	0.9433	29.2949	1.4715	48.5974	1.8353	62.5643	2.1207	73.9078
	0.6	0.0077	0.1905	0.3733	10.3586	0.7017	21.0283	1.2070	39.5113	1.5774	54.2015	1.8705	66.3687
	0.8	0.0051	0.1268	0.2546	6.8097	0.4978	14.2377	0.9269	29.2198	1.2789	42.9825	1.5713	55.2276
	1.0	0.0036	0.0887	0.1797	4.6844	0.3564	9.7958	0.6916	20.7632	0.9944	31.9642	1.2638	42.8335
<i>Sinusoidally distributed load</i>													
5	0.0	0.0158	0.3798	0.6338	18.0329	0.9958	30.0539	1.4525	46.3570	1.7760	58.5463	2.0391	68.7806
	0.2	0.0131	0.3132	0.5622	15.8052	0.9188	27.6207	1.3724	43.9945	1.6886	56.1842	1.9412	66.3525
	0.4	0.0086	0.2049	0.4073	11.0309	0.7295	21.3850	1.1784	37.5949	1.4940	50.0152	1.7428	60.3452
	0.6	0.0055	0.1296	0.2703	6.9968	0.5188	14.4617	0.9260	28.5355	1.2384	40.6386	1.4894	51.0792
	0.8	0.0036	0.0854	0.1815	4.5347	0.3581	9.4848	0.6830	19.8922	0.9637	30.1217	1.2048	39.7251
	1.0	0.0025	0.0593	0.1272	3.1011	0.2531	6.4508	0.4970	13.6998	0.7252	21.3563	0.9351	29.1046
20	0.0	0.0132	0.3639	0.5673	17.9897	0.9251	31.0288	1.3732	48.4600	1.6795	60.9978	1.9206	71.2435
	0.2	0.0111	0.3058	0.5007	15.7108	0.8501	28.3741	1.3019	46.0509	1.6118	58.8559	1.8545	69.2807
	0.4	0.0075	0.2067	0.3612	11.0156	0.6651	21.7013	1.1097	39.0466	1.4270	52.3712	1.6761	63.3102
	0.6	0.0049	0.1342	0.2410	7.1278	0.4680	14.6903	0.8566	29.2710	1.1658	42.0916	1.4182	53.2269
	0.8	0.0033	0.0900	0.1630	4.7134	0.3228	9.7725	0.6234	20.3784	0.8915	30.9239	1.1272	40.9518
	1.0	0.0023	0.0632	0.1148	3.2715	0.2288	6.7474	0.4515	14.1668	0.6635	21.9643	0.8622	29.8852

By introducing a projective weight ζ_A associated with each control point A, the non-uniform ration B-splines (NURBS) basis functions for one and two dimensions can be constructed from the B-splines as follow

$$R_A(\xi) = \frac{N_A(\xi)\zeta_A}{\sum_A^N N_A(\xi)\zeta_A} \tag{32a}$$

$$R_A(\xi, \eta) = \frac{N_A(\xi)M_A(\eta)\zeta_A}{\sum_A^N \sum_A^M N_A(\xi)M_A(\eta)\zeta_A} \tag{32b}$$

As can be seen, the B-splines basis function is a special case of NURBS if all the weights are assigned with an equal constant.

4.2. NURBS-based formulation of microplates with modified couple stress theory

The approximation of the displacement field of a plate in the parametric space can be described as follow

$$\mathbf{u}^h(\xi, \eta) = \sum_A^{n \times m} R_A(\xi, \eta) \mathbf{q}_A, \tag{33}$$

where n and m are the number of control points in the ξ and η directions, respectively, $R_A(\xi, \eta)$ denotes 2-D NURBS basis function. Meanwhile, the vector of nodal degrees of freedom associated with the control point A is given as

$$\mathbf{q}_A = \{ u_{0A} \ v_{0A} \ w_{bA} \ w_{sA} \}^T \tag{34}$$

By substituting the approximation in Eq. (33) into the strains derived in Eqs. (13)–(17), the strain components can be expressed in terms of NURBS as

$$\boldsymbol{\varepsilon}_b = \boldsymbol{\varepsilon}_b^L + \boldsymbol{\varepsilon}_b^{NL} = \sum_A^{n \times m} \left(\mathbf{B}_A^L + \frac{1}{2} \mathbf{B}_A^{NL} \right) \mathbf{q}_A, \tag{35a}$$

$$\boldsymbol{\varepsilon}_s = \sum_A^{n \times m} \mathbf{B}_A^S \mathbf{q}_A, \tag{35b}$$

in which

$$\boldsymbol{\varepsilon}_b^L = \begin{bmatrix} \boldsymbol{\varepsilon}_0^L \\ \boldsymbol{\kappa}_b \\ \boldsymbol{\kappa}_s \end{bmatrix} = \sum_A^{n \times m} \mathbf{B}_A^L \mathbf{q}_A, \quad \boldsymbol{\varepsilon}_b^{NL} = \begin{bmatrix} \boldsymbol{\varepsilon}_0^{NL} \\ \mathbf{0} \\ \mathbf{0} \end{bmatrix} = \frac{1}{2} \sum_A^{n \times m} \mathbf{B}_A^{NL} \mathbf{q}_A, \tag{36}$$

where the linear component and the nonlinear component, which contains the solution \mathbf{q}_A , are respectively defined as

$$\mathbf{B}_A^L = \begin{bmatrix} \mathbf{B}_A^m \\ \mathbf{B}_A^{b1} \\ \mathbf{B}_A^{b2} \end{bmatrix}, \quad \mathbf{B}_A^{NL}(\mathbf{q}) = \begin{bmatrix} \mathbf{A}_\theta \\ \mathbf{0} \\ \mathbf{0} \end{bmatrix} \mathbf{B}_A^g, \tag{37}$$

and the linear gradient matrices are expressed as follows

$$\mathbf{B}_A^m = \begin{bmatrix} R_{A,x} & 0 & 0 & 0 \\ 0 & R_{A,y} & 0 & 0 \\ R_{A,y} & R_{A,x} & 0 & 0 \end{bmatrix}, \quad \mathbf{B}_A^{b1} = - \begin{bmatrix} 0 & 0 & R_{A,xx} & 0 \\ 0 & 0 & R_{A,yy} & 0 \\ 0 & 0 & 2R_{A,xy} & 0 \end{bmatrix},$$

$$\mathbf{B}_A^{b2} = \begin{bmatrix} 0 & 0 & 0 & R_{A,xx} \\ 0 & 0 & 0 & R_{A,yy} \\ 0 & 0 & 0 & 2R_{A,xy} \end{bmatrix}, \tag{38a}$$

$$\mathbf{B}_A^g = \begin{bmatrix} 0 & 0 & R_{A,x} & R_{A,x} \\ 0 & 0 & R_{A,y} & R_{A,y} \end{bmatrix}, \quad \mathbf{B}_A^s = \begin{bmatrix} 0 & 0 & 0 & R_{A,x} \\ 0 & 0 & 0 & R_{A,y} \end{bmatrix}. \tag{38b}$$

Meanwhile, the variation of the strain vectors are derived as

$$\delta \boldsymbol{\varepsilon}_b = \delta \boldsymbol{\varepsilon}_b^L + \delta \boldsymbol{\varepsilon}_b^{NL} = \sum_A^{n \times m} \left(\mathbf{B}_A^L + \mathbf{B}_A^{NL} \right) \delta \mathbf{q}_A \tag{39}$$

Similarly, by substituting the approximation in Eq. (33) into the curvature tensor derived in Eqs. (18) and (19), the curvature tensor components can be obtained as

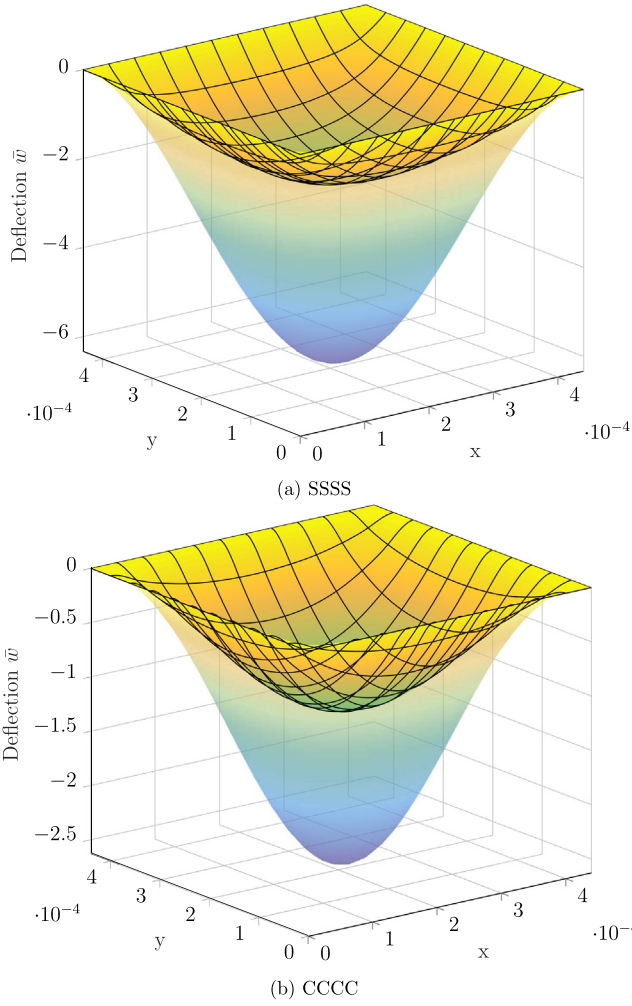


Fig. 10. Linear (outer) and nonlinear (inner) deformed shape of Al/Al₂O₃ square microplates subjected to uniformly distributed load, $a/h = 5, \ell/h = 0.2, n = 1, P = 400$ (rules of mixtures scheme).

$$\chi_b^c = \sum_A^{n \times m} \mathbf{B}_A^{cb} \mathbf{q}_A, \quad (40a)$$

$$\chi_s^c = \sum_A^{n \times m} \mathbf{B}_A^{cs} \mathbf{q}_A, \quad (40b)$$

where

$$\mathbf{B}_A^{cb} = \begin{bmatrix} \tilde{\mathbf{B}}_A^{b0} \\ \tilde{\mathbf{B}}_A^{b1} \end{bmatrix}, \quad \mathbf{B}_A^{cs} = \begin{bmatrix} \tilde{\mathbf{B}}_A^{s0} \\ \tilde{\mathbf{B}}_A^{s2} \end{bmatrix}, \quad (41)$$

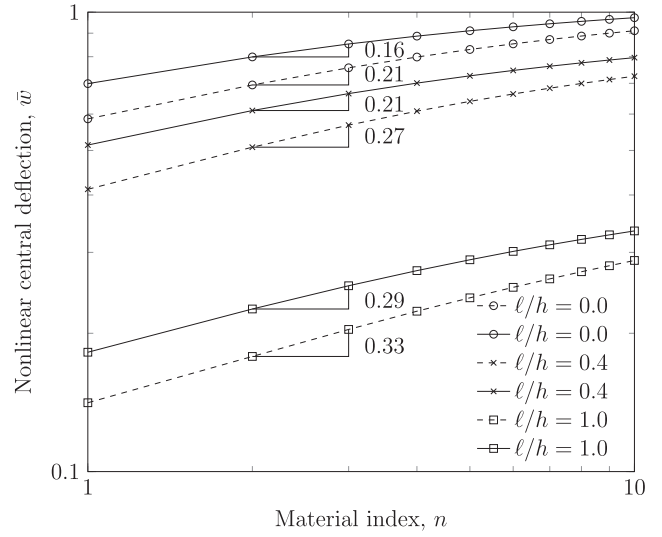
in which

$$\tilde{\mathbf{B}}_A^{b0} = \frac{1}{4} \begin{bmatrix} 0 & 0 & 4R_{A,xy} & 2R_{A,xy} \\ 0 & 0 & -4R_{A,xy} & -2R_{A,xy} \\ 0 & 0 & 2(-R_{A,xx} + R_{A,yy}) & -R_{A,xx} + R_{A,yy} \end{bmatrix}, \quad (42a)$$

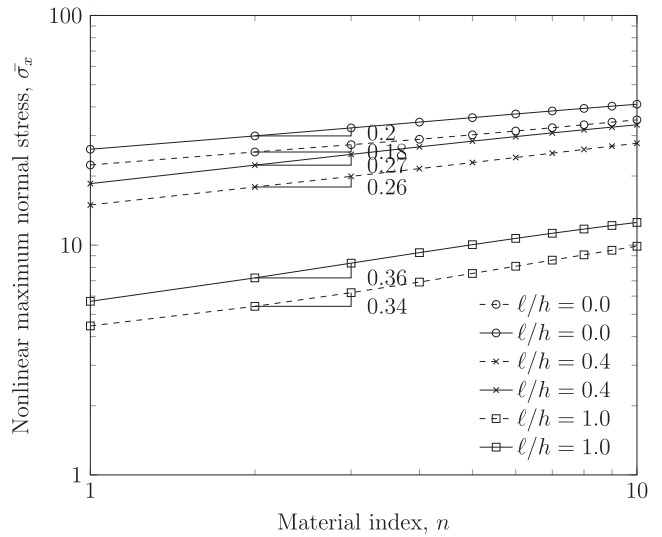
$$\tilde{\mathbf{B}}_A^{b1} = \frac{1}{4} \begin{bmatrix} 0 & 0 & 0 & -2R_{A,xy} \\ 0 & 0 & 0 & 2R_{A,xy} \\ 0 & 0 & 0 & R_{A,xx} - R_{A,yy} \end{bmatrix},$$

$$\tilde{\mathbf{B}}_A^{s0} = \frac{1}{4} \begin{bmatrix} -R_{A,xy} & R_{A,xx} & 0 & 0 \\ -R_{A,yy} & R_{A,xy} & 0 & 0 \end{bmatrix}, \quad \tilde{\mathbf{B}}_A^{s2} = \frac{1}{4} \begin{bmatrix} 0 & 0 & 0 & -R_{A,y} \\ 0 & 0 & 0 & R_{A,x} \end{bmatrix}. \quad (42b)$$

The discretised system of equations for the static analysis is



(a) Nonlinear central deflection $\bar{w}(\frac{a}{2}, \frac{b}{2}, 0)$



(b) Normal stress $\bar{\sigma}_x(\frac{a}{2}, \frac{a}{2}, \frac{h}{2})$

Fig. 11. Effects of material index n and the material length scale ratio ℓ/h on the nonlinear central deflection and normal stress of CCCC Al/Al₂O₃ square microplates, $a/h = 5, P = 100$, with the rules of mixtures scheme (dashed line) and Mori-Tanaka scheme (solid line).

$$\mathbf{K}(\mathbf{q})\mathbf{q} = \mathbf{F}, \quad (43)$$

where the global stiffness matrix is

$$\mathbf{K}(\mathbf{q}) = \mathbf{K}_L + \mathbf{K}_{NL}(\mathbf{q}), \quad (44)$$

in which the global matrices \mathbf{K}_L (linear) and \mathbf{K}_{NL} (nonlinear) are respectively assembled from the element matrices \mathbf{K}_L^e and \mathbf{K}_{NL}^e of the element Ω_e . Those matrices can be expressed as follows

$$\mathbf{K}_L^e = \int_{\Omega_e} (\mathbf{B}_A^L)^T \mathbf{D}^b \mathbf{B}_A^L d\Omega_e + \int_{\Omega_e} (\mathbf{B}_A^S)^T \mathbf{D}^s \mathbf{B}_A^S d\Omega_e + \int_{\Omega_e} (\mathbf{B}_A^{cb})^T \mathbf{D}_c^b \mathbf{B}_A^{cb} d\Omega_e + \int_{\Omega_e} (\mathbf{B}_A^{cs})^T \mathbf{D}_c^s \mathbf{B}_A^{cs} d\Omega_e, \quad (45a)$$

$$\mathbf{K}_{NL}^e(\mathbf{q}) = \int_{\Omega_e} \left(\frac{1}{2} (\mathbf{B}_A^L)^T \mathbf{D}^b \mathbf{B}_A^{NL} + (\mathbf{B}_A^{NL})^T \mathbf{D}^b \mathbf{B}_A^L + \frac{1}{2} (\mathbf{B}_A^{NL})^T \mathbf{D}^b \mathbf{B}_A^{NL} \right) d\Omega_e. \quad (45b)$$

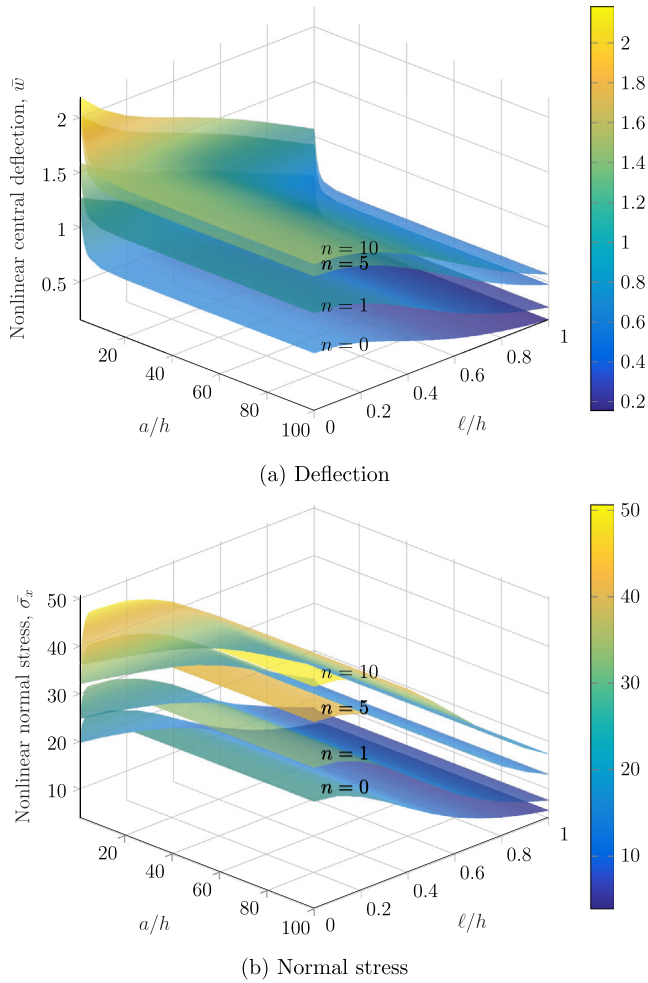


Fig. 12. Variation of nonlinear responses of SSSS Al/Al₂O₃ square microplates with respect to a/h and ℓ/h (rule of mixtures scheme), $P = 100$.

In addition, the load vector is described as

$$\mathbf{F} = \int_{\Omega} q_0 \mathbf{R} d\Omega \quad (46)$$

where

$$\mathbf{R} = [0 \quad 0 \quad R_A \quad R_A]^T \quad (47)$$

It can be inferred from Eqs. (38) and (42) that the second derivatives of the approximation functions are essentially required for the RPT and MCST. These features may cause some difficulties in the traditional FEA, but can be conveniently handled by means of the proposed isogeometric analysis as, by its nature, the derivatives of the basis functions could be derived easily and naturally. In addition, the system of equations includes the nonlinear term \mathbf{q} on the left-hand side of the Eq. (43), which contains unknown control variables. As a result, an iterative approach should be considered to solve such a problem.

4.3. Newton-Raphson iterative procedure

In the Newton-Raphson procedure, the nonlinear equation in Eq. (43) is solved iteratively in which the solutions of the unknowns in the previous step are used to solve for the solution in the current step. These iterations are performed until the solution converges. Following these ideas, the residual force vector is defined as

$$\tilde{\mathbf{R}}(\mathbf{q}) = \mathbf{K}(\mathbf{q})\mathbf{q} - \mathbf{F} = (\mathbf{K}_L + \mathbf{K}_{NL}(\mathbf{q}))\mathbf{q} - \mathbf{F}. \quad (48)$$

Then the improved solution at the end of the $(i + 1)^{th}$ iteration is calculated as

$${}^{i+1}\mathbf{q} = {}^i\mathbf{q} + \Delta\mathbf{q}, \quad (49)$$

where the incremental displacement $\Delta\mathbf{q}$ is given by

$$\Delta\mathbf{q} = \frac{-\tilde{\mathbf{R}}({}^i\mathbf{q})}{\mathbf{K}_T}, \quad (50)$$

in which the tangent stiffness matrix \mathbf{K}_T can be obtained by [65]

$$\mathbf{K}_T = \frac{\partial \tilde{\mathbf{R}}({}^i\mathbf{q})}{\partial \mathbf{q}} = \mathbf{K}_L + \tilde{\mathbf{K}}_{NL} + \mathbf{K}_g, \quad (51)$$

where the nonlinear matrix

$$\tilde{\mathbf{K}}_{NL}(\mathbf{q}) = \int_{\Omega} \left((\mathbf{B}_A^L)^T \mathbf{D}^b \mathbf{B}_A^{NL} + (\mathbf{B}_A^{NL})^T \mathbf{D}^b \mathbf{B}_A^L + (\mathbf{B}_A^{NL})^T \mathbf{D}^b \mathbf{B}_A^{NL} \right) d\Omega, \quad (52)$$

and the geometric stiffness matrix

$$\mathbf{K}_g = \int_{\Omega} (\mathbf{B}^g)^T \begin{bmatrix} N_x & N_{xy} \\ N_{xy} & N_y \end{bmatrix} \mathbf{B}^g d\Omega, \quad (53)$$

where \mathbf{B}^g is assembled from \mathbf{B}_A^g in Eq. (38). The iterations are executed until the difference between the solutions from two consecutive iterations is no greater than the predefined tolerance ϵ as described below

$$\frac{\|{}^{i+1}\mathbf{q} - {}^i\mathbf{q}\|}{\|{}^{i+1}\mathbf{q}\|} \leq \epsilon. \quad (54)$$

5. Numerical examples

In this section, the numerical results of the nonlinear bending analysis of square, circular and annular plates will be shown. The convergence and verification are firstly presented to demonstrate the validity and efficiency of the proposed IGA approach for nonlinear problems of plate structures without and with size effects. For the analysis of microplates with small-scale effects, the material length scale parameter ℓ , unless otherwise specified, is assigned the value of 17.6×10^{-6} m as suggested by Lam et al. [1]. It should be noted that $\ell/h = 0$ implies no size effect is taken into account. In these investigations, the plates which are made of isotropic material and FGMs with mixtures of ceramic and metal shown in Table 1 are used. The geometries of square, circular and annular plates employed in this study are printed in Fig. 3. It should be noted that, for verification and comparison purposes, the material properties could be different units or without specific unit. For the efficient presentation of the results, the following normalised formula, unless otherwise specified, are used:

$$P = \frac{q_0 a^4}{E_m h^4}; \quad \bar{w} = \frac{w}{h}; \quad \bar{\sigma}_x = \frac{\sigma_x a^2}{E_m h^2} \quad (55)$$

5.1. Convergence and verification studies

In order to illustrate the validity and the convergence of the proposed IGA approach and refined plate formulation for nonlinear plate problems with MCST in Section 4, a number of numerical tests have been conducted to deal with the nonlinear bending of isotropic and FG plates. Fig. 4 presents the convergence rate of the numerical results toward the analytical solution of Levy [66] whose work is widely considered as a standard reference for nonlinear problems. The analytical reference result is calculated for

Table 7Normalised deflection $\bar{w}(0, 0, 0)$ and normal stress $\bar{\sigma}_x(0, 0, \frac{h}{2})$ of circular Al/ZnO₂ microplates subjected to uniformly distributed load (rule of mixtures scheme, $n = 5$).

h/R	ℓ/h	$P = 1$		$P = 50$		$P = 100$		$P = 200$		$P = 300$		$P = 400$	
		\bar{w}	$\bar{\sigma}_x$	\bar{w}	$\bar{\sigma}_x$	\bar{w}	$\bar{\sigma}_x$	\bar{w}	$\bar{\sigma}_x$	\bar{w}	$\bar{\sigma}_x$	\bar{w}	$\bar{\sigma}_x$
<i>Simply-supported (SSSS, as defined in Reddy et al. [28])</i>													
0.1	0.0	0.3784	1.6354	2.2122	16.6821	2.8106	24.6444	3.5582	36.8432	4.0809	46.8473	4.4966	55.6639
	0.2	0.3722	1.5920	2.2111	16.6896	2.8104	24.6581	3.5585	36.8576	4.0813	46.8609	4.4971	55.6771
	0.4	0.3593	1.4988	2.2083	16.7038	2.8102	24.6960	3.5597	36.9028	4.0829	46.9057	4.4989	55.7212
	0.6	0.3469	1.4084	2.2044	16.7095	2.8098	24.7454	3.5616	36.9742	4.0856	46.9810	4.5020	55.7970
	0.8	0.3372	1.3397	2.2000	16.7014	2.8095	24.7941	3.5641	37.0604	4.0893	47.0794	4.5061	55.8996
	1.0	0.3302	1.2912	2.1957	16.6838	2.8087	24.8329	3.5668	37.1499	4.0934	47.1900	4.5110	56.0201
0.5	0.0	0.4267	1.5608	2.2035	15.8369	2.8018	23.6692	3.5523	35.6463	4.0776	45.4525	4.4954	54.0875
	0.2	0.4194	1.5340	2.2025	15.8886	2.8010	23.7431	3.5515	35.7505	4.0768	45.5786	4.4945	54.2319
	0.4	0.4040	1.4780	2.1999	16.0138	2.7992	23.9233	3.5499	36.0026	4.0750	45.8845	4.4925	54.5829
	0.6	0.3878	1.4219	2.1967	16.1518	2.7974	24.1289	3.5483	36.2909	4.0734	46.2341	4.4908	54.9839
	0.8	0.3737	1.3744	2.1935	16.2643	2.7962	24.3087	3.5479	36.5466	4.0729	46.5443	4.4902	55.3388
	1.0	0.3621	1.3354	2.1905	16.3435	2.7954	24.4455	3.5485	36.7516	4.0739	46.7943	4.4913	55.6260
<i>Fully clamped</i>													
0.1	0.0	0.1383	0.7522	2.0564	15.8791	2.6894	23.3494	3.4603	34.8581	3.9910	44.3909	4.4102	52.8501
	0.2	0.1237	0.6708	2.0281	15.7718	2.6675	23.2474	3.4428	34.7002	3.9760	44.1830	4.3975	52.6031
	0.4	0.0937	0.5053	1.9436	15.3597	2.6037	22.9318	3.3945	34.3111	3.9344	43.6818	4.3595	51.9965
	0.6	0.0667	0.3573	1.8018	14.4121	2.4955	22.2610	3.3141	33.7041	3.8664	42.9934	4.2989	51.2052
	0.8	0.0475	0.2532	1.6082	12.8063	2.3398	21.0101	3.1965	32.7197	3.7685	42.0473	4.2124	50.2166
	1.0	0.0346	0.1842	1.3810	10.7284	2.1391	19.0814	3.0398	31.1718	3.6368	40.6652	4.0962	48.8840
0.5	0.0	0.2722	0.8742	2.1483	14.4573	2.7480	22.0957	3.4935	33.8540	4.0127	43.5197	4.4249	52.0503
	0.2	0.2318	0.7562	2.1289	14.2221	2.7341	21.8094	3.4837	33.5119	4.0050	43.1440	4.4187	51.6510
	0.4	0.1604	0.5263	2.0690	13.7115	2.6901	21.2063	3.4516	32.7902	3.9784	42.3508	4.3953	50.8085
	0.6	0.1051	0.3422	1.9669	12.9403	2.6141	20.4143	3.3948	31.8821	3.9314	41.3505	4.3532	49.7263
	0.8	0.0707	0.2283	1.8198	11.7611	2.5022	19.3106	3.3116	30.7626	3.8612	40.1648	4.2914	48.4734
	1.0	0.0497	0.1597	1.6318	10.1762	2.3529	17.7840	3.1994	29.3084	3.7670	38.7067	4.2082	46.9825

clamped isotropic square plates with aspect ratio $a/h = 100$ subjected to uniform loading. This figure includes convergences of normalised nonlinear central deflection of clamped isotropic plates (Material I) with different element meshes, ranging from 3 to 17 elements per edge, and element polynomial orders, $p = 2, 3$ and 4. As expected, while the quadratic elements ($p = 2$) show slower convergence rate and less accuracy, the higher-order elements ($p = 3$ or $p = 4$) yield better performance in terms of convergences and differences compared to the analytical solution [66]. Having pointed out in the work of Nguyen et al. [63], the meshes of 11×11 cubic ($p = 3$) elements with total of 784 degrees of freedom which are sufficient in between accuracy and computational cost will be used. Table 2 shows the complete comparison of the presented numerical linear and nonlinear results of square isotropic plates with those of other researchers including Levy's analytical solution [66], Pica et al.'s FEM with Mindlin formulation [67], Kant and Kommineni's C⁰ FEM with high-order formulation [68], Urthaler and Reddy's mixed FEM [69], and Kapoor and Kapania's IGA with first-order formulation [57]. It can be observed that, for all cases of load parameter P , the present solutions are in good agreement with the analytical solutions and other published results for both normalised deflection and normal stress. For better illustration of the accuracy of the proposed method and differences of linear and nonlinear solutions, all results are plotted in the Fig. 5.

The validity and accuracy of the proposed IGA with RPT is further investigated for FG square plates. Fig. 6 depicts the comparison of the nonlinear central deflection of simply-supported (SSSS) square plates subjected to uniformly distributed load. The plates are made of Al/ZnO₂ in which the material properties are assumed to follow the rule of mixtures. The proposed results with different values of material index n are compared to those of Praveen and Reddy [70] using FEM based on 5-DOF FSDT and Phung-Van et al. [58] employing cell-based smoothed three-node plate elements based on 7-DOF HSDT. As can be seen, the presented results are quite close to the others', especially the former one. This

confirms the accuracy and validity of the proposed approach which is applicable not only for isotropic plates but also for the FG plates.

Figs. 7 and 8 depict the bending behaviours including central deflection and normal stress of simply-supported and fully clamped FG microplates with size effects, respectively. The presented results, that are generated from different values of material length scale ratio ℓ/h and material index n , are compared with those reported by Kim and Reddy [29] who employed general third-order theory for element formulation of FG microplates. It is observed that the solutions of the two approaches are in excellent agreement although there are small discrepancy in central displacements of clamped microplates with relatively high material length scale ratio ($\ell/h = 0.5$ and 1). It is worth commenting that Kim and Reddy [29] employed the general third-order shear deformation plate theory (GTPT) with 11 unknowns and 16×16 meshes of conforming cubic elements to analyse the microplates. Meanwhile, the RPT with only 4 variables and meshes of 11×11 cubic elements are used in this study. The comparison of the computational efforts in terms of total number of DOFs between the reference and present approaches is provided in Table 3. As can be seen, for a single analysis, the reference approach requires over 16 times as many DOFs as the present approach does. For the nonlinear analysis in which iterative procedures are involved, the difference between the two approaches in terms of computational cost becomes much more significant. As a result, IGA approach performs far better than that of FEM doing in these specific nonlinear problems.

The accuracy of the proposed approach is further demonstrated for circular plates in Fig. 9 where the proposed solutions are almost coincident with the results published by Reddy et al. [28] for various boundary conditions and material parameters. It should be noted that for the analysis of circular plates, unless otherwise specified, the constrained DOFs of simply-supported boundary conditions are indicated similar to those presented in the work of Reddy et al. [28]. Generally, the positive outcomes confirm the

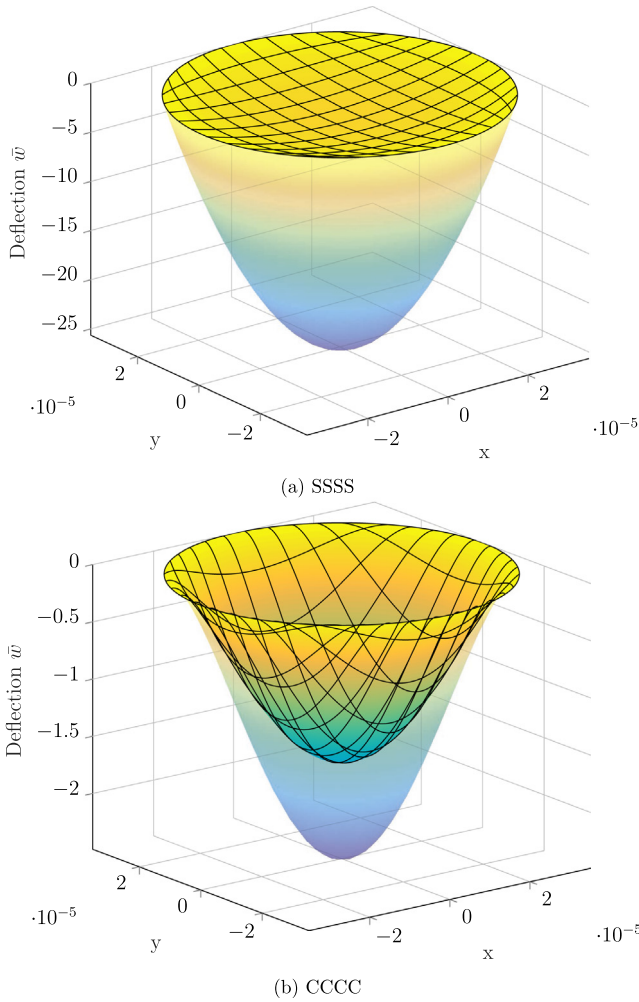
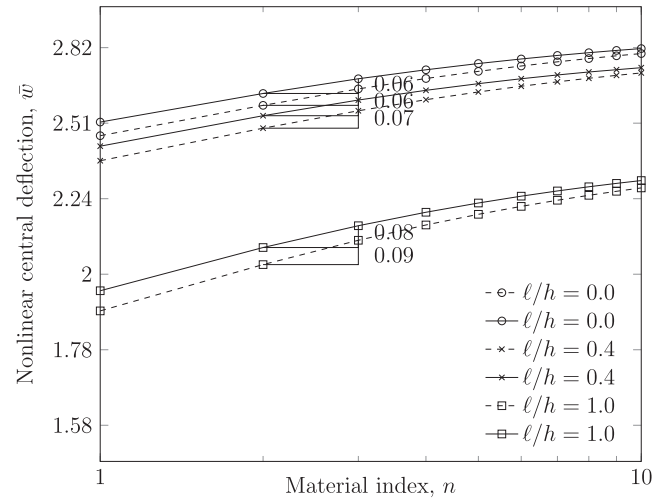


Fig. 13. Linear (outer) and nonlinear (inner) deformed shape of Al/ZnO₂ circular microplates subjected to uniformly distributed load, $h/R = 0.5, \ell/h = 1, n = 5, P = 50$ (rules of mixtures scheme).

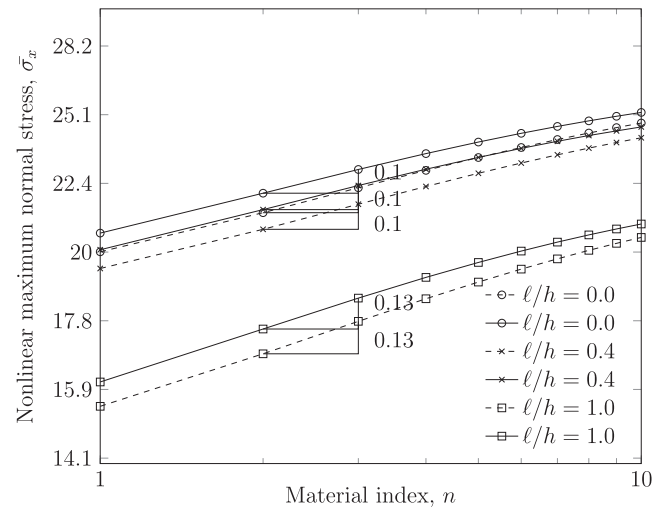
accuracy and validity of the proposed method regardless of material properties, structure scales and geometries.

5.2. Nonlinear analysis of square microplates

In this part, a number of numerical studies of the nonlinear behaviour of square FG microplates is conducted to demonstrate the effects of aspect ratio a/h , material length scale ratio ℓ/h , material index n and load parameter P . Tables 4 and 5 present the normalised central deflection and normal stress of simply-supported and fully clamped square Al/Al₂O₃ microplates in which the rule of mixtures is employed to model the material distribution through the thickness. The plates are subjected to either uniformly distributed load, q_0 , or sinusoidally distributed load, $q_0 \sin(\frac{\pi x}{a}) \sin(\frac{\pi y}{a})$. The results are generated for different values of $a/h, \ell/h$ and P , while keeping material index $n = 1$. Similarly, the numerical results for SSSS microplates, which employ the Mori-Tanaka scheme for material modelling, are provided in Table 6. These results which have not been reported before could serve as the benchmark examples for the future references. For illustration purposes, Fig. 10 depicts the deformed shapes of square microplates under uniform load with different boundary conditions. As can be seen, being placed together in the same plots, the nonlinear displacements are always smaller than those of linear counterparts. The reason for this phenomenon is that the nonlinear analy-



(a) Nonlinear central deflection $\bar{w}(\frac{a}{2}, \frac{b}{2}, 0)$



(b) Normal stress $\bar{\sigma}_x(\frac{a}{2}, \frac{b}{2}, 0)$

Fig. 14. Effects of the material index n and the material length scale ratio ℓ/h on the nonlinear central deflection and normal stress of fully clamped Al/ZnO₂ circular microplates, $h/R = 0.2, P = 100$, with the rules of mixtures scheme (dashed line) and Mori-Tanaka scheme (solid line).

sis takes into account the low and higher order terms of the strains while the linear analysis only considers the first order ones. This additional consideration contributes to the increase of the strain energy and the stiffness of the structure correspondingly, which results in smaller displacements for nonlinear cases as presented.

The effects of material index n and material length scale ratio ℓ/h on the nonlinear central deflection and normal stress of fully clamped Al/Al₂O₃ square microplates with different material distribution models are plotted in Fig. 11. The results are generated for the plates with aspect ratio $a/h = 5$ and load parameter $P = 100$ and with different values of ℓ/h of 0.0, 0.4, 1.0. It can be observed that the increase of material index n is followed by the increase of central displacement. However, the growth of material length scale ratio ℓ/h leads to a completely different scenario in which the displacement is declined. It is worth commenting that these phenomena are due to the increase of structure stiffness as the material length scale ratio ℓ/h becomes smaller causing the displacement to reduce as expected. In other words, for a specific material length scale ℓ , the thinner the microplate is, the higher the stiffness becomes. For further illustration, Fig. 12 presents

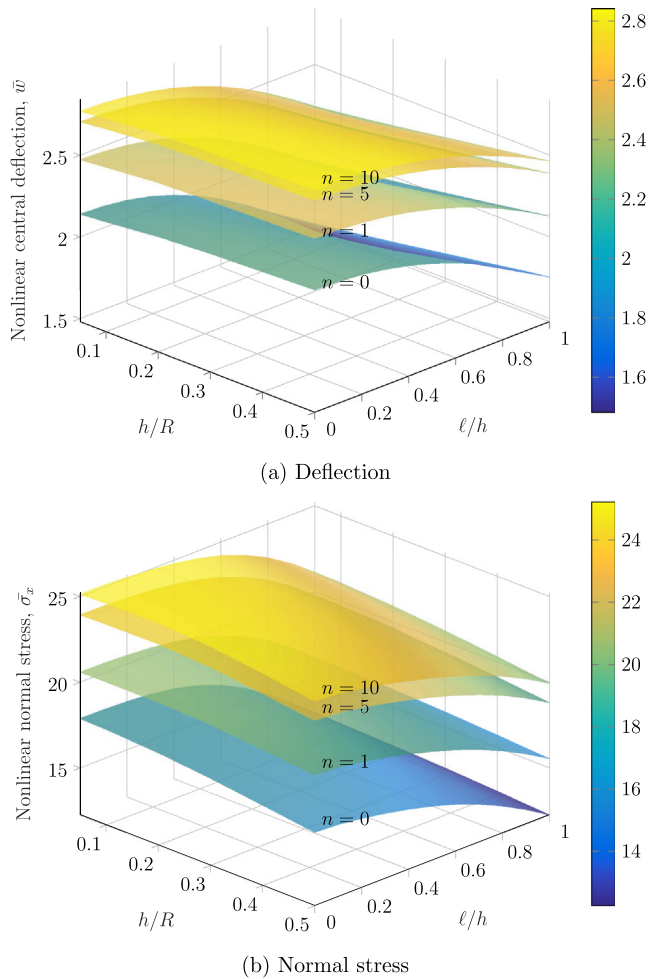


Fig. 15. Variation of nonlinear responses of fully clamped Al/ZnO₂ circular microplates with respect to h/R and ℓ/h (Mori-Tanaka scheme), $P = 100$.

the variation of nonlinear deflection and normal stress of simply-supported Al/Al₂O₃ square microplates in which the plate's aspect ratio a/h and material length scale ratio ℓ/h are taken into account. As can be seen, the influence of the aspect ratio a/h on the bending responses is remarkable for thin square plates ($a/h \leq 10$). However, it becomes less pronounced as the square plates get thicker.

5.3. Nonlinear analysis of circular microplates

A number of investigations on the nonlinear bending behaviours of circular FG microplates will be presented in this part of the section. Table 7 shows the normalised deflection and normal stress of circular Al/ZnO₂ microplates subjected to uniform loading in which the material distribution follows the rule of mixtures. The results are generated for both simply-supported and fully clamped boundary conditions with various values of aspect ratio a/h , material length scale ratio ℓ/h and load parameter P . Since there is no published report for this problem of nonlinear analysis of FG circular microplates, these numerical results can serve as a benchmark example for future references. Fig. 13 provides a visual illustration of the deformed shapes of circular Al/ZnO₂ microplates in which the solutions for linear and nonlinear problems are placed together. The solutions are generated for the specific material and geometry inputs with different boundary conditions.

Fig. 14 illustrates the effect of the material index n and material length scale ratio ℓ/h on the nonlinear deflection and normal stress

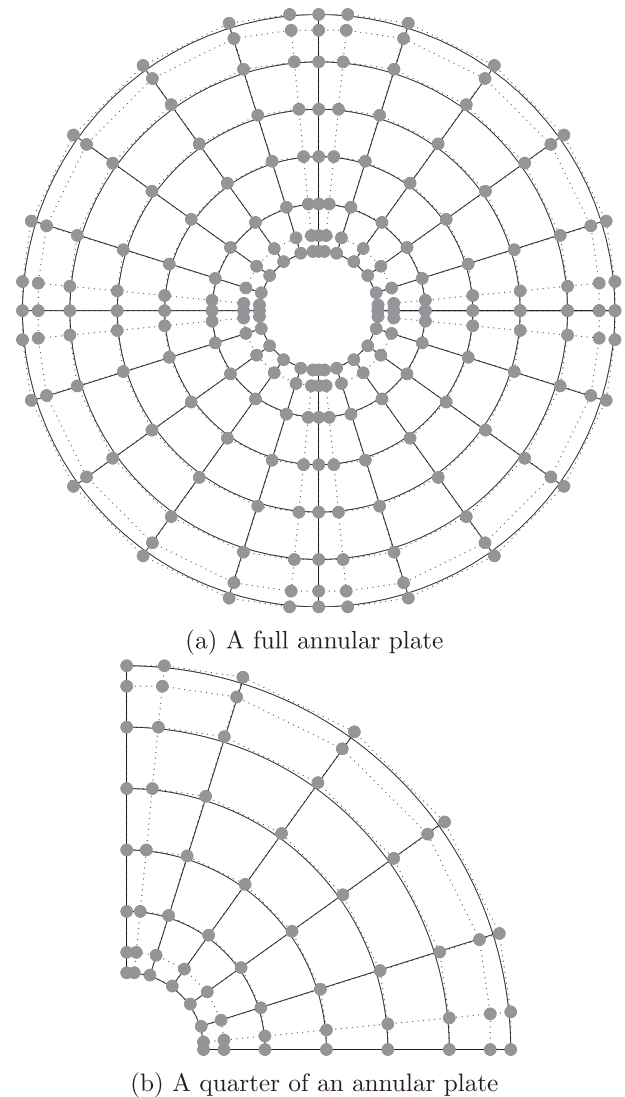
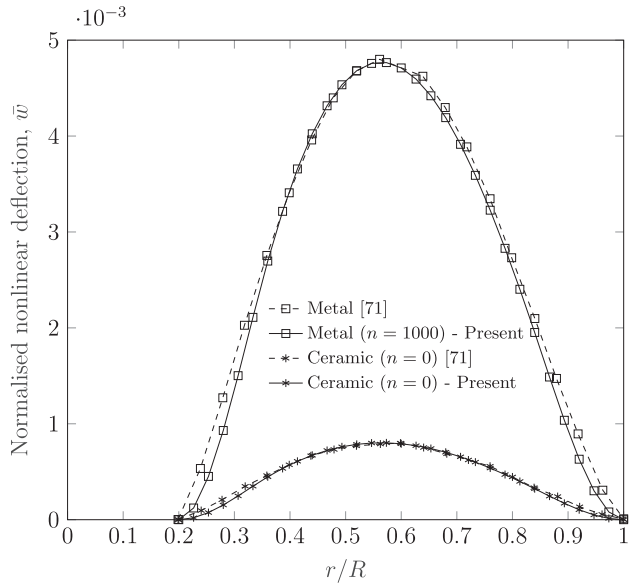


Fig. 16. Element mesh (solid line), control point (grey dot) and control point net (dotted line).

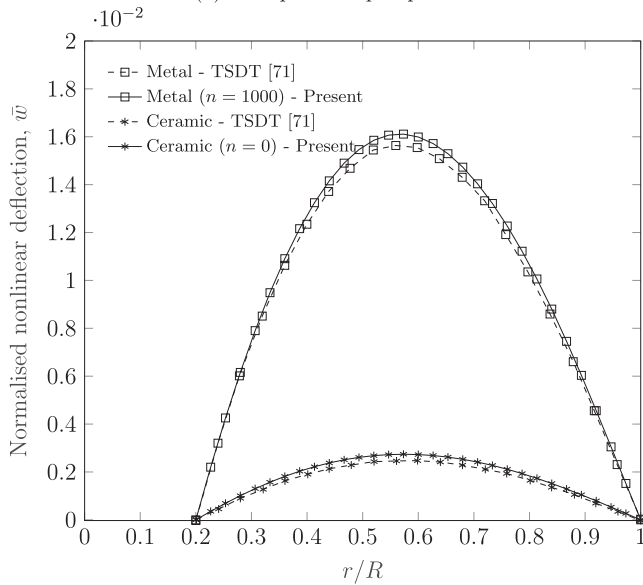
of fully clamped Al/ZnO₂ circular microplates with different material distribution schemes. Similarly to the square microplates, the decline of material index n and the increase of material length scale ratio ℓ/h lead to the strengthening of the plates' stiffness. Consequently, the displacement and normal stress of the plates are both decreased accordingly. However, while the influence of the square plates' aspect ratio a/h on its bending behaviours are different for thin and thick plates, those impacts of the circular plates' aspect ratio h/R on the displacement and normal stress responses remain less pronounced regardless of plates' geometry as shown in Fig. 15.

5.4. Nonlinear analysis of annular microplates

In this part of the section, a number of analyses are conducted to assess the nonlinear bending behaviours of the annular microplates. The full geometry configuration and element meshes along with control point net of the annular are presented in Fig. 3c and Fig. 16, respectively. Due to its symmetry, for the sake of computational effort, only a quarter of this cut-out geometry is used for the analysis. The nonlinear bending responses of the annular microplates without considering size effects are compared with the



(a) Clamped-clamped plate



(b) Simply-supported plate

Fig. 17. Comparison of nonlinear deflection through radius of Al/SiC annular plates, $h/R = 0.15$.

results reported by Golmakani and Kadkhodayan [71]. As can be observed from Fig. 17, the results generated from this proposed approach agree well with those published which are based on TSDT theory and the finite difference technique for both fully clamped and simply-supported boundary conditions which are applied at inner and outer circles of the annular microplates.

In order to show the effects of the material length scale to nonlinear bending behaviours of annular microplates, the variations of the vertical displacement through the radius are shown in Fig. 18. As expected, when the size-dependent effects are considered, the displacement of the microplate becomes smaller reaching its lowest as the material length scale ratio $\ell/h = 1$. Fig. 19 illustrates the deformed shapes of annular microplates for both linear and nonlinear bending cases with same geometry, material and loading inputs. Similarly to other geometries, the linear analysis predicts larger deflections than that of nonlinear case in which von Kármán strains are involved.

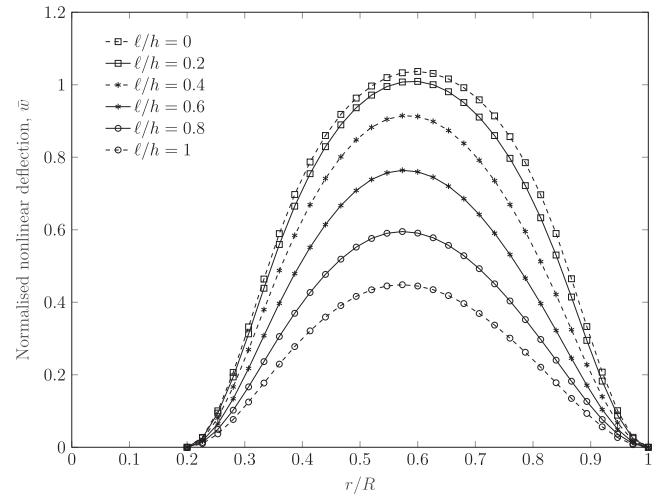


Fig. 18. Normalised deflection of CC Al/SiC annular microplates, $h/R = 0.3, n = 0, P = 600$.

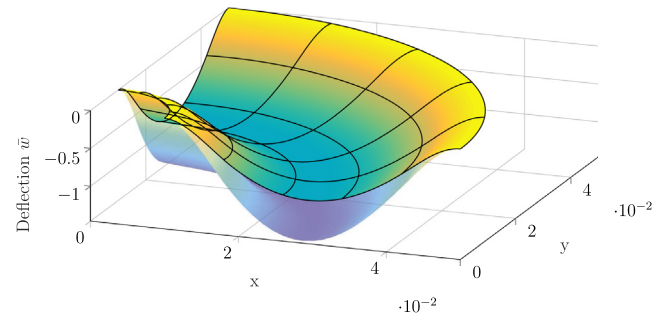


Fig. 19. Linear (outer) and nonlinear (inner) deformed shapes of Al/SiC annular microplates subjected to uniformly distributed load, $h/R = 0.15, \ell/h = 0.2, n = 0, P = 600$.

6. Conclusions

The isogeometric analysis associated with the four-unknown refined plate theory is proposed to investigate the geometrically nonlinear bending responses of small-scale FG plates. The refined plate theory which requires C^1 elements is used to construct the displacement fields before the nonlinear von Kármán strains are derived. Meanwhile, the size-dependent effects are efficiently captured by the MCST in which only length scale parameter is involved. While the NURBS-based isogeometric analysis is successfully implemented to construct higher-order elements which are essentially required in refined plate and modified couple stress theories, the solutions of nonlinear problems are reliably obtained by means of Newton-Raphson iterative procedure. A number of convergence and verification studies confirm the validity and reliability of the proposed RPT-based IGA approach which is highly robust compared to other HSDT-based FEA approaches in terms of computational efforts including the number of unknowns and element meshes. Besides, some benchmark results for nonlinear bending analysis have been presented which can be used for future references. Parametric studies are also presented, which show that the inclusion of material length scale causes the stiffness of the continuum to increase, especially when the material length scale ratio ℓ/h gets larger. Consequently, the nonlinear displacements and stresses of microplates decline. Meanwhile, the increase of material index n leads to a completely different scenario in which the displacements are also risen. In addition, although the

influence of the aspect ratio a/h on the bending responses is remarkable for thin plates, it turns less pronounced when the thick plates are considered.

Acknowledgement

The first and last authors gratefully acknowledge the financial support from the Northumbria University via the Researcher Development Framework. The first author would also like to acknowledge the supports from the Santander Universities Mobility Grant and Prof. E. Atroshchenko for the research visit at the University of Chile in March 2017.

References

- [1] Lam D, Yang F, Chong A, Wang J, Tong P. Experiments and theory in strain gradient elasticity. *J Mech Phys Solids* 2003;51(8):1477–508. [http://dx.doi.org/10.1016/S0022-5096\(03\)00053-X](http://dx.doi.org/10.1016/S0022-5096(03)00053-X).
- [2] Fu Y, Du H, Huang W, Zhang S, Hu M. TiNi-based thin films in MEMS applications: a review. *Sensors Actuat. A: Phys.* 2004;112(23):395–408. <http://dx.doi.org/10.1016/j.sna.2004.02.019>.
- [3] Lee Z, Ophus C, Fischer LM, Nelson-Fitzpatrick N, Westra KL, Evoy S, et al. Metallic NEMS components fabricated from nanocomposite AlMo films. *Nanotechnology* 2006;17(12):3063. <http://dx.doi.org/10.1088/0957-4484/17/12/042>.
- [4] Baughman RH, Cui C, Zakhidov AA, Iqbal Z, Barisci JN, Spinks GM, et al. Carbon nanotube actuators. *Science* 1999;284(5418):1340–4. <http://dx.doi.org/10.1126/science.284.5418.1340>.
- [5] Lau K-T, Cheung H-Y, Lu J, Yin Y-S, Hui D, Li H-L. Carbon nanotubes for space and bio-engineering applications. *J Comput Theor Nanosci* 2008;5(1):23–35. <http://dx.doi.org/10.1166/jctn.2008.003>.
- [6] Mindlin RD. Influence of couple-stresses on stress concentrations. *Exp Mech* 1963;3(1):1–7. <http://dx.doi.org/10.1007/BF02327219>.
- [7] Mindlin RD. Micro-structure in linear elasticity. *Arch Ration Mech Anal* 1964;16(1):51–78. <http://dx.doi.org/10.1007/BF00248490>.
- [8] Mindlin RD. Second gradient of strain and surface-tension in linear elasticity. *Int J Solids Struct* 1965;1(4):417–38. [http://dx.doi.org/10.1016/0020-7683\(65\)90006-5](http://dx.doi.org/10.1016/0020-7683(65)90006-5).
- [9] Mindlin RD, Tiersten HF. Effects of couple-stresses in linear elasticity. *Arch Ration Mech Anal* 1962;11(1):415–48. <http://dx.doi.org/10.1007/BF00253946>.
- [10] Eringen AC. Nonlocal polar elastic continua. *Int J Eng Sci* 1972;10(1):1–16. [http://dx.doi.org/10.1016/0020-7225\(72\)90070-5](http://dx.doi.org/10.1016/0020-7225(72)90070-5).
- [11] Eringen AC, Edelen DGB. On nonlocal elasticity. *Int J Eng Sci* 1972;10(3):233–48. [http://dx.doi.org/10.1016/0020-7225\(72\)90039-0](http://dx.doi.org/10.1016/0020-7225(72)90039-0).
- [12] Reddy JN, Srinivasa AR. Non-linear theories of beams and plates accounting for moderate rotations and material length scales. *Int J Non-Linear Mech* 2014;66:43–53. <http://dx.doi.org/10.1016/j.iinonlinmec.2014.06.003>.
- [13] Reddy JN. Nonlocal nonlinear formulations for bending of classical and shear deformation theories of beams and plates. *Int J Eng Sci* 2010;48(11):1507–18. <http://dx.doi.org/10.1016/j.iinengsci.2010.09.020>.
- [14] Fleck NA, Muller GM, Ashby MF, Hutchinson JW. Strain gradient plasticity: theory and experiment. *Acta Metall Mater* 1994;42(2):475–87. [http://dx.doi.org/10.1016/0956-7151\(94\)90502-9](http://dx.doi.org/10.1016/0956-7151(94)90502-9).
- [15] Fleck NA, Hutchinson JW. A phenomenological theory for strain gradient effects in plasticity. *J Mech Phys Solids* 1993;41(12):1825–57. [http://dx.doi.org/10.1016/0022-5096\(93\)90072-N](http://dx.doi.org/10.1016/0022-5096(93)90072-N).
- [16] Toupin RA. Theories of elasticity with couple-stress. *Arch Ration Mech Anal* 1964;17(2):85–112. <http://dx.doi.org/10.1007/BF00253050>.
- [17] Yang F, Chong ACM, Lam DCC, Tong P. Couple stress based strain gradient theory for elasticity. *Int J Solids Struct* 2002;39(10):2731–43. [http://dx.doi.org/10.1016/S0020-7683\(02\)00152-X](http://dx.doi.org/10.1016/S0020-7683(02)00152-X).
- [18] Chen J, Li C-J. A quadrilateral spline element for couple stress/strain gradient elasticity. *Comput Struct* 2014;138:133–41. <http://dx.doi.org/10.1016/j.compstruct.2014.03.006>.
- [19] Park SK, Gao X-L. Bernoulli-Euler beam model based on a modified couple stress theory. *J Micromech Microeng* 2006;16(11):2355. <http://dx.doi.org/10.1088/0960-1317/16/11/015>.
- [20] Park SK, Gao X-L. Variational formulation of a modified couple stress theory and its application to a simple shear problem. *Zeitschrift für angewandte Mathematik und Physik* 2008;59(5):904–17. <http://dx.doi.org/10.1007/s00033-006-6073-8>.
- [21] Roque CMC, Fidalgo DS, Ferreira AJM, Reddy JN. A study of a microstructure-dependent composite laminated Timoshenko beam using a modified couple stress theory and a meshless method. *Compos Struct* 2013;96:532–7. <http://dx.doi.org/10.1016/j.compstruct.2012.09.011>.
- [22] Salamat-talab M, Nateghi A, Torabi J. Static and dynamic analysis of third-order shear deformation FG micro beam based on modified couple stress theory. *Int J Mech Sci* 2012;57(1):63–73. <http://dx.doi.org/10.1016/j.iijmesci.2012.02.004>.
- [23] Trinh LC, Nguyen HX, Vo TP, Nguyen T-K. Size-dependent behaviour of functionally graded microbeams using various shear deformation theories based on the modified couple stress theory. *Compos Struct* 2016;154:556–72. <http://dx.doi.org/10.1016/j.compstruct.2016.07.033>.
- [24] Tsiatas GC. A new Kirchhoff plate model based on a modified couple stress theory. *Int J Solids Struct* 2009;46(13):2757–64. <http://dx.doi.org/10.1016/j.ijsolstr.2009.03.004>.
- [25] Yin L, Qian Q, Wang L, Xia W. Vibration analysis of microscale plates based on modified couple stress theory. *Acta Mech Solida Sin* 2010;23(5):386–93. [http://dx.doi.org/10.1016/S0894-9166\(10\)60040-7](http://dx.doi.org/10.1016/S0894-9166(10)60040-7).
- [26] Ma HM, Gao X-L, Reddy JN. A non-classical Mindlin plate model based on a modified couple stress theory. *Acta Mech* 2011;220(1–4):217–35. <http://dx.doi.org/10.1007/s00707-011-0480-4>.
- [27] Thai H-T, Vo TP. A size-dependent functionally graded sinusoidal plate model based on a modified couple stress theory. *Compos Struct* 2013;96:376–83. <http://dx.doi.org/10.1016/j.compstruct.2012.09.025>.
- [28] Reddy JN, Romanoff J, Loya JA. Nonlinear finite element analysis of functionally graded circular plates with modified couple stress theory. *Eur J Mech A Solids* 2016;56:92–104. <http://dx.doi.org/10.1016/j.euromechsol.2015.11.001>.
- [29] Kim J, Reddy JN. A general third-order theory of functionally graded plates with modified couple stress effect and the von Kármán nonlinearity: theory and finite element analysis. *Acta Mech* 2015;226(9):2973–98. <http://dx.doi.org/10.1007/s00707-015-1370-y>.
- [30] Su H, Banerjee JR. Development of dynamic stiffness method for free vibration of functionally graded Timoshenko beams. *Comput Struct* 2015;147:107–16. <http://dx.doi.org/10.1016/j.compstruc.2014.10.001>.
- [31] Trinh LC, Vo TP, Osofero AI, Lee J. Fundamental frequency analysis of functionally graded sandwich beams based on the state space approach. *Compos Struct* doi:<http://dx.doi.org/10.1016/j.compstruct.2015.11.010>.
- [32] Thai CH, Kulasegaram S, Tran LV, Nguyen-Xuan H. Generalized shear deformation theory for functionally graded isotropic and sandwich plates based on isogeometric approach. *Comput Struct* 2014;141:94–112. <http://dx.doi.org/10.1016/j.compstruc.2014.04.003>.
- [33] Mantari JL, Soares CG. A quasi-3d tangential shear deformation theory with four unknowns for functionally graded plates. *Acta Mech* 2014;226(3):625–42. <http://dx.doi.org/10.1007/s00707-014-1192-3>.
- [34] Fantuzzi N, Brischetto S, Tornabene F, Viola E. 2d and 3d shell models for the free vibration investigation of functionally graded cylindrical and spherical panels. *Compos Struct* 2016;154:573–90. <http://dx.doi.org/10.1016/j.compstruct.2016.07.076>.
- [35] Reddy JN. A simple higher-order theory for laminated composite plates. *J Appl Mech* 1984;51(4):745–52. <http://dx.doi.org/10.1115/1.3167719>.
- [36] Soldatos KP. A transverse shear deformation theory for homogeneous monoclinic plates. *Acta Mech* 1992;94(3–4):195–220. <http://dx.doi.org/10.1007/BF01176650>.
- [37] Senthilnathan NR, Lim SP, Lee KH, Chow ST. Buckling of shear-deformable plates. *AIAA J* 1987;25(9):1268–71. <http://dx.doi.org/10.2514/3.48742>.
- [38] Reddy JN, Kim J. A nonlinear modified couple stress-based third-order theory of functionally graded plates. *Compos Struct* 2012;94(3):1128–43. <http://dx.doi.org/10.1016/j.compstruct.2011.10.006>.
- [39] Reddy JN, Berry J. Nonlinear theories of axisymmetric bending of functionally graded circular plates with modified couple stress. *Compos Struct* 2012;94(12):3664–8. <http://dx.doi.org/10.1016/j.compstruct.2012.04.019>.
- [40] Zhang B, He Y, Liu D, Gan Z, Shen L. A non-classical Mindlin plate finite element based on a modified couple stress theory. *Eur J Mech A Solids* 2013;42:63–80. <http://dx.doi.org/10.1016/j.euromechsol.2013.04.005>.
- [41] Thai H-T, Kim S-E. A size-dependent functionally graded Reddy plate model based on a modified couple stress theory. *Compos Part B: Eng* 2013;45(1):1636–45. <http://dx.doi.org/10.1016/j.compositesb.2012.09.065>.
- [42] He L, Lou J, Zhang E, Wang Y, Bai Y. A size-dependent four variable refined plate model for functionally graded microplates based on modified couple stress theory. *Compos Struct* 2015;130:107–15. <http://dx.doi.org/10.1016/j.compstruct.2015.04.033>.
- [43] Hughes T, Cottrell J, Bazilevs Y. Isogeometric analysis: Cad, finite elements, nurbs, exact geometry and mesh refinement. *Comput Meth Appl Mech Eng* 2005;194(3941):4135–95. <http://dx.doi.org/10.1016/j.cma.2004.10.008>.
- [44] Lee C-K, Angela Mihai L, Hale JS, Kerfriden P, Bordas SPA. Strain smoothing for compressible and nearly-incompressible finite elasticity. *Comput Struct* 2017;182:540–55. <http://dx.doi.org/10.1016/j.compstruct.2016.05.004>.
- [45] Cottrell JA, Hughes TJR, Bazilevs Y. *Isogeometric analysis: toward integration of CAD and FEA*. 1st ed. Wiley Publishing; 2009.
- [46] Vuong AV, Heinrich C, Simeon B. ISOGAT: A 2d tutorial MATLAB code for Isogeometric Analysis. *Comput Aided Geomet Des* 2010;27(8):644–55. <http://dx.doi.org/10.1016/j.cagd.2010.06.006>.
- [47] de Falco C, Reali A, Vazquez R. GeOPDEs: A research tool for Isogeometric Analysis of PDEs. *Adv Eng Softw* 2011;42(12):1020–34. <http://dx.doi.org/10.1016/j.advengsoft.2011.06.010>.
- [48] Nguyen VP, Anitescu C, Bordas SPA, Rabczuk T. Isogeometric analysis: an overview and computer implementation aspects. *Math Comput Simul* 2015;117:89–116. <http://dx.doi.org/10.1016/j.matcom.2015.05.008>.
- [49] Nguyen-Xuan H, Tran LV, Thai CH, Kulasegaram S, Bordas S. Isogeometric analysis of functionally graded plates using a refined plate theory. *Compos Part B: Eng* 2014;64:222–34. <http://dx.doi.org/10.1016/j.compositesb.2014.04.001>.

- [50] Beiro da Veiga L, Buffa A, Lovadina C, Martinelli M, Sangalli G. An isogeometric method for the ReissnerMindlin plate bending problem. *Comput Meth Appl Mech Eng* 2012;209(212):45–53. <http://dx.doi.org/10.1016/j.cma.2011.10.009>.
- [51] Tran LV, Thai CH, Nguyen-Xuan H. An isogeometric finite element formulation for thermal buckling analysis of functionally graded plates. *Finite Elem Anal Des* 2013;73:65–76. <http://dx.doi.org/10.1016/j.finel.2013.05.003>.
- [52] Thai S, Thai H-T, Vo TP, Patel VI. Size-dependant behaviour of functionally graded microplates based on the modified strain gradient elasticity theory and isogeometric analysis. *Comput Meth Appl Mech Eng* 2010;199(58):276–89. <http://dx.doi.org/10.1016/j.compstruc.2017.05.014>.
- [53] Kiendl J, Bletzinger KU, Linhard J, Wchner R. Isogeometric shell analysis with KirchhoffLove elements. *Comput Meth Appl Mech Eng* 2009;198(4952):3902–14. <http://dx.doi.org/10.1016/j.cma.2009.08.013>.
- [54] Benson DJ, Bazilevs Y, Hsu MC, Hughes TJR. Isogeometric shell analysis: the ReissnerMindlin shell. *Comput Meth Appl Mech Eng* 2010;199(58):276–89. <http://dx.doi.org/10.1016/j.cma.2009.05.011>.
- [55] Nguyen-Thanh N, Kiendl J, Nguyen-Xuan H, Wchner R, Bletzinger KU, Bazilevs Y, et al. Rotation free isogeometric thin shell analysis using PHT-splines. *Comput Meth Appl Mech Eng* 2011;200(4748):3410–24. <http://dx.doi.org/10.1016/j.cma.2011.08.014>.
- [56] Tornabene F, Fantuzzi N, Baccocchi M. The GDQ method for the free vibration analysis of arbitrarily shaped laminated composite shells using a NURBS-based isogeometric approach. *Compos Struct* 2016;154:190–218. <http://dx.doi.org/10.1016/j.compstruct.2016.07.041>.
- [57] Kapoor H, Kapania RK. Geometrically nonlinear NURBS isogeometric finite element analysis of laminated composite plates. *Compos Struct* 2012;94(12):3434–47. <http://dx.doi.org/10.1016/j.compstruct.2012.04.028>.
- [58] Phung-Van P, Nguyen-Thoi T, Luong-Van H, Lieu-Xuan Q. Geometrically nonlinear analysis of functionally graded plates using a cell-based smoothed three-node plate element (CS-MIN3) based on the CO-HSDT. *Comput Meth Appl Mech Eng* 2014;270:15–36. <http://dx.doi.org/10.1016/j.cma.2013.11.019>.
- [59] Tran LV, Lee J, Nguyen-Van H, Nguyen-Xuan H, Wahab MA. Geometrically nonlinear isogeometric analysis of laminated composite plates based on higher-order shear deformation theory. *Int J Non-Linear Mech* 2015;72:42–52. <http://dx.doi.org/10.1016/j.ijnonlinmec.2015.02.007>.
- [60] Chong ACM, Yang F, Lam DCC, Tong P. Torsion and bending of micron-scaled structures. *J Mater Res* 2001;16(4):1052–8. <http://dx.doi.org/10.1557/JMR.2001.0146>.
- [61] Nakamura T, Wang T, Sampath S. Determination of properties of graded materials by inverse analysis and instrumented indentation. *Acta Mater* 2000;48(17):4293–306. [http://dx.doi.org/10.1016/S1359-6454\(00\)00217-2](http://dx.doi.org/10.1016/S1359-6454(00)00217-2).
- [62] Mori T, Tanaka K. Average stress in matrix and average elastic energy of materials with misfitting inclusions. *Acta Metall* 1973;21(5):571–4. [http://dx.doi.org/10.1016/0001-6160\(73\)90064-3](http://dx.doi.org/10.1016/0001-6160(73)90064-3).
- [63] Nguyen HX, Nguyen TN, Abdel-Wahab M, Bordas SPA, Nguyen-Xuan H, Vo TP. A refined quasi-3d isogeometric analysis for functionally graded microplates based on the modified couple stress theory. *Comput Meth Appl Mech Eng* 2017;313:904–40. <http://dx.doi.org/10.1016/j.cma.2016.10.002>.
- [64] Reddy JN. An introduction to nonlinear finite element analysis. OUP Oxford; 2004.
- [65] Nguyen-Van H. Development and application of assumed strain smoothing finite element technique for composite plate/shell structures [Ph.D. thesis]. University of Southern Queensland; 2009.
- [66] Levy S. Square plate with clamped edges under normal pressure producing large deflections, Tech. Rep. 740, National Advisory Committee for Aeronautics, Jan. 1942. <<http://ntrs.nasa.gov/search.jsp?R=19930091819>>.
- [67] Pica A, Wood RD, Hinton E. Finite element analysis of geometrically nonlinear plate behaviour using a mindlin formulation. *Comput Struct* 1980;11(3):203–15. [http://dx.doi.org/10.1016/0045-7949\(80\)90160-1](http://dx.doi.org/10.1016/0045-7949(80)90160-1).
- [68] Kant T, Kommineni JR. CO Finite element geometrically non-linear analysis of fibre reinforced composite and sandwich laminates based on a higher-order theory. *Comput Struct* 1992;45(3):511–20. [http://dx.doi.org/10.1016/0045-7949\(92\)90436-4](http://dx.doi.org/10.1016/0045-7949(92)90436-4).
- [69] Urthaler Y, Reddy JN. A mixed finite element for the nonlinear bending analysis of laminated composite plates based on FSDT. *Mech Adv Mater Struct* 2008;15(5):335–54. <http://dx.doi.org/10.1080/15376490802045671>.
- [70] Praveen GN, Reddy JN. Nonlinear transient thermoelastic analysis of functionally graded ceramic-metal plates. *Int J Solids Struct* 1998;35(33):4457–76. [http://dx.doi.org/10.1016/S0020-7683\(97\)00253-9](http://dx.doi.org/10.1016/S0020-7683(97)00253-9).
- [71] Golmakani ME, Kadkhodayan M. Nonlinear bending analysis of annular FGM plates using higher-order shear deformation plate theories. *Compos Struct* 2011;93(2):973–82. <http://dx.doi.org/10.1016/j.compstruct.2010.06.024>.